Main Manuscript for

Sp140L Is a Novel Herpesvirus Restriction Factor

Jana M. Cable[1], Wiyada Wongwiwat[2], Jenna C. Grabowski[1], Robert E. White[2*], Micah A. Luftig[1*]

[1]Duke University School of Medicine, Department of Molecular Genetics and Microbiology, Duke Center for Virology, Durham, NC, USA

[2]Section of Virology, Department of Infectious Disease, Imperial College London, London, United Kingdom

*Co-corresponding authors

Emails: micah.luftig@duke.edu; robert.e.white@imperial.ac.uk

Author Contributions: M.A.L., R.E.W., and J.M.C. designed research, J.M.C., W.W., J.G., and R.E.W., performed research, J.M.C., W.W., J.G., R.E.W., and M.A.L. analyzed data, J.M.C., R.E.W., and M.A.L. wrote the paper.

Preprint servers: BioRxiv

Competing Interest Statement: The authors declare not competing interest.

Classification: Biological Sciences, Microbiology

Keywords: Herpesvirus, Speckled Proteins, PML Nuclear Bodies, DNA sensing, Epstein-Barr virus

This PDF file includes:

Main Text

Abstract

Herpesviruses, including Epstein-Barr Virus (EBV) – a human oncogenic viruses and essential trigger of multiple sclerosis, must bypass host DNA sensing mechanisms to establish lifelong, latent infection. Therefore, herpesviruses encode viral proteins to disrupt key host factors involved in DNA sensing and viral restriction. The first viral latency protein expressed, EBNA-LP, is essential for transformation of naïve B cells and establishment of viral gene expression, yet its role in evading host defenses remains unclear. Using single-cell RNA sequencing of EBNA-LP-Knockout (LPKO)-infected B cells, we reveal an antiviral response landscape implicating the 'speckled proteins' as key cellular restriction factors countered by EBNA-LP. Specifically, loss of *SP100* or the primate-specific *SP140L* reverses the restriction of LPKO, suppresses a subset of canonically interferon-stimulated genes, and restores transcription of essential latent viral genes and cellular proliferation. Notably, we also identify Sp140L as a restriction target of the herpesvirus saimiri ORF3 protein, implying a role for Sp140L in immunity to other diverse DNA viruses. This study reveals Sp140L as a restriction factor that we propose links sensing and transcriptional suppression of viral DNA to an IFN-independent innate immune response, likely relevant to all nuclear DNA viruses.

Significance Statement

Herpesviruses, including the oncogenic Epstein-Barr virus (EBV), are restricted by DNA sensing during initial infection and therefore encode viral proteins to antagonize key restriction factors. We found that the EBV latency protein EBNA-LP, disrupts the 'speckled proteins' Sp100 and Sp140L - an evolutionarily recent protein with unknown function, which we find promotes an anti-viral state that suppresses cellular proliferation, characterized by high induction of cellular anti-viral genes and suppressed transcription of essential viral latency genes. Sp140L also restricts the herpesvirus saimiri, which we find antagonizes Sp140L through the viral protein ORF3. Our study therefore identifies Sp140L as a novel restriction factor of diverse herpesviruses, and likely all DNA viruses, during a critical stage of initial viral infection.

Main Text

Introduction

Herpesviruses are double stranded DNA viruses that cause lifelong infections due to their ability to establish viral latency and avoid immunodetection (1). Clinically relevant herpesviruses include herpes simplex virus (HSV), human cytomegalovirus (HCMV) and Kaposi's sarcoma associated herpesvirus (KSHV), as well as Epstein-Barr virus (EBV), which is associated with numerous lymphomas and carcinomas, and is implicated in several autoimmune disorders – particularly multiple sclerosis (2-4). The B cell biology of EBV infection and associated diseases can be modeled *in vitro,* as infection of primary B cells leads to cellular transformation and the generation of immortalized lymphoblastoid cell lines (LCLs). Given the ability of herpesviruses to

62 establish lifelong latency, initial infection is a crucial stage where cellular sensing and restriction
63 can prevent the virus from successfully establishing latency. Yet, the mechanisms of intrinsic
64 restriction of herpesviruses have not been fully elucidated.

65 One key mediator of defense against DNA viruses are PML nuclear bodies (PML-NBs),
66 membrane-less nuclear compartments involved in the intrinsic DNA sensing and epigenetic
67 repression of viral chromatin through loading repressive histones and epigenetic modifications on
68 the incoming naked viral DNA genomes (5, 6). Components of PML-NBs can also play a role in the
69 innate antiviral response through inducing expression of interferon-stimulated genes (ISGs) (7-12).
70 Core PML-NB proteins implicated in restricting DNA viruses include PML, DAXX, ATRX, and Sp100.
71 PML serves as a scaffold to mediate the interaction of other core proteins, while DAXX and ATRX
72 together load the repressive histone variant H3.3 onto viral genomes during initial infection -
73 preventing the accumulation of active histone marks on the incoming viral genome and suppressing
74 the transcription of viral genes (13-17). HIRA, a separate histone chaperone complex recruited to
75 PML-NBs upon herpesvirus infection (17) and IFN treatment (8, 17), also contributes to H3.3
76 deposition on viral chromatin in HSV infection (17, 18). In contrast, H3.3 loading by HIRA at ISG
77 gene loci activates gene expression (7, 8). The speckled protein Sp100, can restrict the replication
78 and viral gene expression of the DNA viruses HSV (19, 20), HCMV(21), Human Papilloma Virus
79 (22), and adenovirus (23) when these viruses lack effective countermeasures or when their
80 countermeasures are species-mismatched. Sp100 can bind the heterochromatin protein HP1α (24)
81 and can localize to the promoters of ISGs upon IFN stimulation (10). However, the mechanisms
82 by which Sp100 restricts DNA virus infection is still unclear.

83 Beyond *SP100*, the speckled protein genetic locus includes additional family members
84 *SP110*, *SP140*, and – exclusively in primates – *SP140L* (25), whose roles in viral infection are
85 largely unknown. The speckled family genes all encode four key domains: i) an N-terminal caspase
86 recruitment (CARD) domain (previously called heterogeneously staining region – HSR) involved in
87 multimerization, ii) the DNA-binding (SAND) "Sp100, AIRE, NucP41/P75 and DEAF" domain, iii) a
88 methyl-histone-binding plant homeodomain (PHD) domain, and iv) a C-terminal acetyl-lysine-
89 binding bromodomain (BRD) (25). Genetic mutations in *SP110* and *SP140* are associated with
90 autoimmune disorders and increased susceptibility to intracellular bacterial infections (25). And
91 while Sp110 and Sp140 repress the Type I IFN response in mice (26, 27), they appear to promote
92 Type I IFN responses in humans (28). The *SP140L* gene arose as a likely meiotic crossover event
93 between the *SP100* and *SP140* genes, resulting in a gene combining the 5' CARD domain-
94 encoding region of *SP100* and the remaining protein-encoding domains of the *SP140* gene (29).
95 The function of Sp140L, however, remains unexplored.

96 To overcome PML-NB restriction, successful herpesviruses encode proteins that
97 antagonize various PML-NB components of their hosts. These include viral tegument proteins
98 belonging to the viral FGARAT homolog family, such as pp71 in HCMV (30, 31) and BNRF1 in EBV

99 (32) which target DAXX and ATRX; ORF75 in KSHV which antagonizes DAXX, ATRX, PML, and
100 Sp100 (33), and ORF3 of Herpesvirus Saimiri (HVS) – a KSHV-like rhadinovirus of squirrel
101 monkeys – which degrades Sp100 (34). Some immediate-early viral proteins also antagonize PML-
102 NBs, including ICP0 in HSV - a viral E3 ubiquitin ligase which targets PML, Sp100, DAXX, and
103 ATRX (35, 36); IE1 in HCMV targeting PML and Sp100 (21, 37); and EBNA-LP in EBV, which
104 transiently displaces Sp100 from PML-NBs during early infection (38, 39). While the molecular
105 mechanism by which these viral proteins antagonize PML-NB components may be distinct, the
106 functional consequences are similar as evidenced by the ability of ICP0 or various combinations of
107 BNRF1 or pp71 with IE1 or EBNA-LP to complement an ICP0-null HSV and pp71-deficient HCMV
108 (40-42). The role of Sp100 in EBV infection has not been directly investigated, with studies largely
109 limited to using transient transfection rather than primary infection systems (38, 39), and focusing
110 on the shortest Sp100 isoform – Sp100A – which does not contain the SAND, PHD, or Bromo
111 domains, and promotes viral gene transcription, whereas the longer Sp100 isoforms restrict DNA
112 viruses (23, 43).
113 EBNA-LP is critical for the transformation of naïve B cells by EBV infection(44), but its
114 function in early infection is not well defined compared to other PML-NB-disrupting herpesvirus
115 proteins mentioned above. The architecture of EBNA-LP is unique in that it is composed of N-
116 terminal, identical, 66 amino acid repeats (W domains) and a C-terminal 45 amino acid Y domain.
117 While the structure of EBNA-LP is unknown, it is predicted to be highly disordered(45). Based on
118 transient transfection assays, EBNA-LP was thought to primarily function as a co-activator of
119 another early EBV protein, EBNA2 to enhance expression of the essential viral gene Latent
120 Membrane Protein 1 (LMP1) and some cellular genes (46-50). The mechanism by which EBNA-LP
121 co-activates EBNA2 has been variously attributed to displacement of the transcriptionally
122 repressive HDAC4 and NCoR proteins from viral and cellular promoters (51, 52). However, B cells
123 infected with an EBNA-LP Knockout EBV (LPKO) exhibit reduced expression of not only LMP1, but
124 also other viral genes that are not EBNA2-dependent, while EBNA2-induced host gene expression
125 is not reduced, or even increased, in the absence of EBNA-LP during infection(44) suggesting that
126 EBNA-LP's relationship to EBNA2 is more complex than a simple 'coactivator'. Additionally, our
127 recent work identified highly conserved, hydrophobic leucine-rich motifs in both the W and Y
128 domains of EBNA-LP that associate with the DNA-looping factor YY1 (53). Thus, EBNA-LP likely
129 has EBNA2-independent roles that are critical for establishing latency in, and transformation of,
130 naïve B cells.
131 Given the essential role of immediate-early herpesvirus proteins in overcoming intrinsic
132 viral restriction, and particularly the gap in knowledge as to how and why EBNA-LP is necessary
133 for EBV infection and transformation of naïve B cells, we used single cell RNA-sequencing
134 (scRNAseq) to compare the trajectories of wild type (WT) and LPKO virus infected B cells during
135 the first days of infection. This assay revealed key facets of the restriction of EBV in the absence

136 of EBNA-LP. We then defined the cellular factors and mechanisms responsible for the restriction of
137 the LPKO virus, and finally the breadth of how these factors are restrictive across human DNA
138 viruses.
139
140 **Results**
141 **EBNA-LP Dictates the Fate Trajectories of EBV-Infected B Cells**
142 To assess the role of EBNA-LP in EBV-driven B cell fate trajectories, we performed single
143 cell RNA sequencing (scRNAseq) of primary human B cells prior to infection (Day 0), and at 2, 5,
144 and 8 days following WT and LPKO infection as depicted in **Fig. 1A**. B cell purity (**Fig. S1A**) and
145 infection efficiency (**Fig. S1B**) were confirmed by expression of CD19 and CD23 respectively at
146 time of collection. Single cell RNA-seq revealed that infected samples contained more mRNA (**Fig.**
147 **S1C**) and more unique mRNA features (**Fig. S1D**) per cell than uninfected (Day 0) B cells.
148 Dimensional reduction integrating all seven samples generated a single UMAP for further analysis
149 (**Fig. 1B**). Uninfected cells largely cluster separately from infected cells (**Fig. 1C**) and 2 days post-
150 infection LPKO- and WT-infected clusters are nearly identical to each other (**Fig. S1D and S1E**).
151 Differences in cellular states between WT- and LPKO-infected B cells emerge by 5 days (**Fig. S1F**
152 **and S1G**) and are accentuated 8 days post-infection (**Fig. S1H and S1I**).

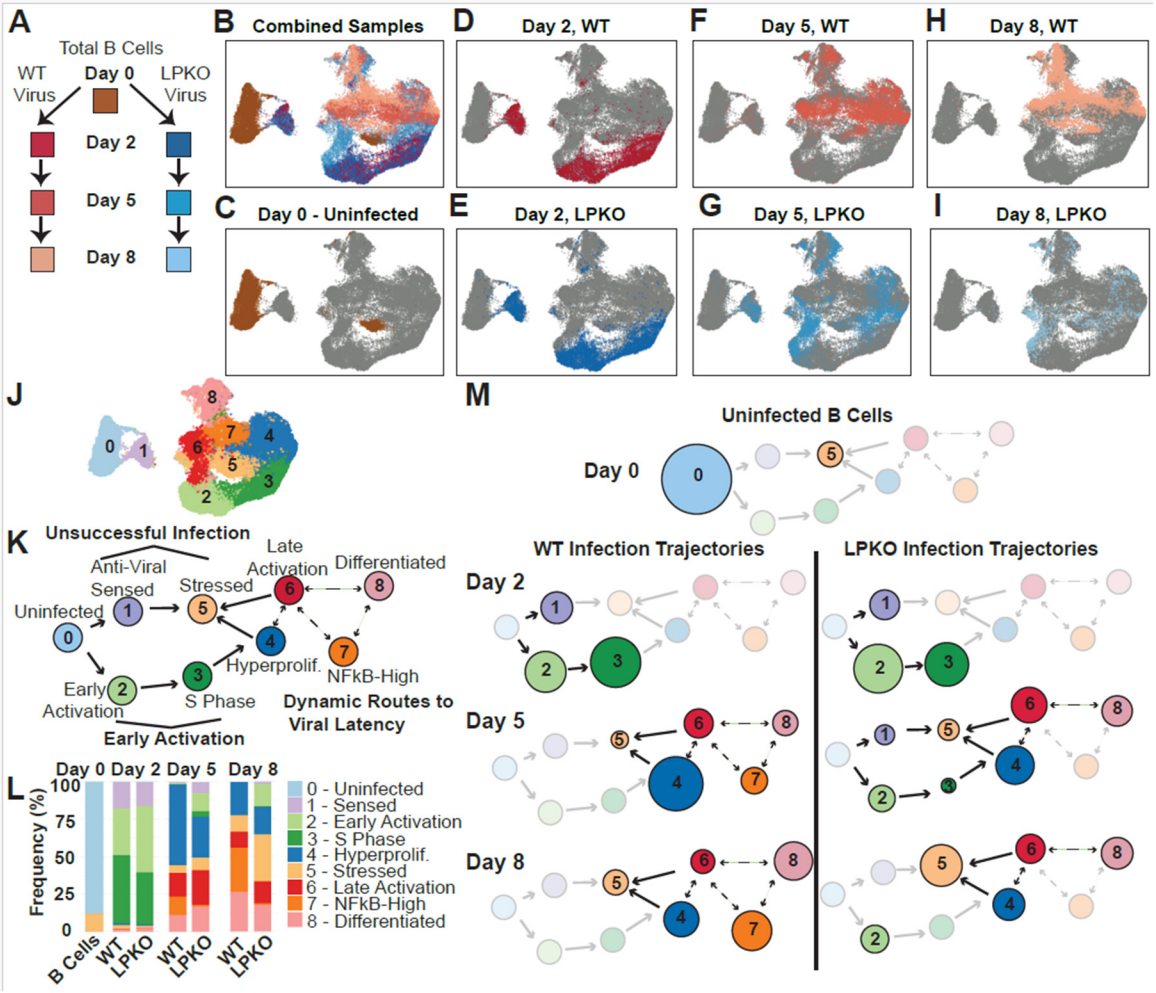

Fig. 1. LPKO-infected B cells have altered cellular trajectories compared to WT EBV. (**A**) Schematic of collected samples. (**B**) Uniform Manifold Approximation and Project for Dimension Reduction (UMAP) of the combined seven samples. Colors correspond to samples in (**A**). (**C**) UMAP with uninfected B cells highlighted. (**D**) Cells 2 days post-infection with WT. (**E**) Cells 2 days post-infection with LPKO. (**F**) Cells 5 days post-infection with WT. (**G**) Cells 5 days post-infection LPKO. (**H**) Cells 8 days post-infection WT. (**I**) Cells 8 days post-infection LPKO. (**J**) UMAP with cells grouped into 9 unique clusters based on differential gene expression. (**K**) Model of the identified clusters in the cellular trajectories of EBV infected B cells. (**L**) Frequency of each cluster within each sample. (**M**) Model of the trajectories of WT- and LPKO-infected B cells at each time point based on frequencies in (**L**). Circle area is proportional to frequency of cluster in each sample. Transparent circles represent clusters which are absent.

Our prior work defined a set of distinct B cell fate trajectories following EBV infection that largely mimic the states of B cell activation and germinal center maturation(54). In comparing WT- and LPKO-infected cells, we have identified 9 distinct cell states that largely recapitulated those characterized previously (**Fig. 1J and Table S1**). We used the top cluster-defining genes in our previous study to identify the corresponding cell states in this dataset (**Fig. S2A-S2I**). Cell states were further distinguished on the basis of viral gene expression (**Fig. S2J-S2U**) and cell cycle phase (**Fig. S2V-S2X**). Cluster 0 (Uninfected – c0) contained uninfected naïve and memory B cells

173 (**Fig. 1K**). Two days post-infection, prior to cellular proliferation, which begins around 3 days post-
174 infection (55), a portion of cells exist in a gene expression state associated with antiviral sensing
175 (Sensed – c1) (**Fig. 1K**). Cells that avoid this initial barrier transition towards an activated state,
176 resembling pre-germinal center B cells (Early Activation – c2), and towards a state of DNA
177 replication enriched for cells in S phase (S Phase – c3) (**Fig. 1K**). By 5 days post-infection, cells
178 advanced to a state of hyperproliferation, with markers of dark zone germinal center B cells
179 (Hyperproliferating – c4) (**Fig. 1K**). Likely as a result of the cellular stress associated with EBV-
180 induced hyperproliferation (55, 56), by this time point some cells also arrest in a state of cellular
181 stress (Stressed – c5) (**Fig. 1K**). Cells also transition towards a second, but distinct, activated B
182 cell state (Late Activation – c6) (**Fig. 1K**). Compared to the Early Activation state (c2), this Late
183 Activation state (c6) is more highly enriched in naïve B cells based on IgD expression (**Fig. S2X**),
184 has lower expression of Myc and E2F targets (**Fig. S2Y and S2Z**) likely a consequence of reduced
185 expression of the viral transactivator EBNA2 in c6 compared to c2 (57) (**Fig. S2R**), and is likely
186 dependent upon cells having undergone proliferation based on its appearance only after day 2 (**Fig.
187 1K**). EBV-infected cells also enter a NFκB-High state, likely driven by the viral protein LMP1, whose
188 expression is highest in this population (**Fig. S2T**), that is characterised by markers of light zone
189 germinal center B cells (NFκB High - c7) (**Fig. 1K**). The final population is a differentiated
190 plasmablast-like state (Differentiated - c8) (**Fig. 1K**).
191 While this model held true for WT-infected cells, LPKO-infected cells had altered
192 trajectories. First, unlike WT-infected cells, LPKO-infected cells remain in the early (pre-proliferation)
193 states of activation (c2 and c3) beyond 2 days post infection (**Fig. 1L**). Second, LPKO-infected cells
194 were also more likely than WT-infected cells to enter states of antiviral sensing (c1) or cellular stress
195 (c5) after day 2 (**Fig. 1L**). Finally, the LPKO-infected cells largely failed to establish the NFκB-High
196 state (c7) (**Fig. 1L**), consistent with the previously reported low expression of LMP1 in LPKO
197 infections (44) (**Fig. S2U**). Surprisingly, the LPKO virus efficiently established the plasmablast state
198 (Differentiated – c8) (**Fig. 1L**), despite the absence of the NFκB-High state which is critical in the
199 emergence of plasmablasts from the germinal center (58). Interpreted as trajectories in **Fig. 1M**,
200 LPKO-infected cells persist in early infection states of activation (c2 and c3) and cellular stress prior
201 to proliferation (c1) longer than WT. LPKO-infected cells that do hyperproliferate, have a higher
202 propensity to arrest with signs of cellular stress (c5) and to enter a germinal center- or light zone-
203 independent route towards the plasmablast state (c8), similar to germinal center-independent B
204 cell maturation (59).
205 To validate our transcriptome data, we first identified RNA changes in cell surface markers
206 defining the key cell populations. RNA levels of CCR6 (**Fig. 2A**) and CD23 (**Fig. 2B**) in the scRNA-
207 seq data distinguish many cell states, similar to previous studies(54). Early Activation states (c2
208 and c3) are characterized by $CCR6^{hi/}CD23^{lo}$ expression, while the Late Activation state (c6) is
209 $CCR6^{hi/}CD23^{hi}$. The NFκB-High state (c7) is $CCR6^{lo}/CD23^{hi}$ and is further resolved by high

expression of ICAM1 (**Fig. 2C**), a proxy marker for LMP1 expression (60). The remaining states are CCR6^{lo}/CD23^{lo} with the Stressed (c5) distinguishable from the Differentiated state (c8) by low expression of CD38 (**Fig. 2D**) and reduced cellular proliferation. Therefore, these markers along with the proliferation tracker CellTrace should allow quantitation of the main states that differ between LPKO and WT infections: persistence in states of activation (c2, c3, c6), reduced transition to the NFκB-high state (c7), and increased cellular arrest prior to hyperproliferation (c5) as outlined in **Fig. 2E**.

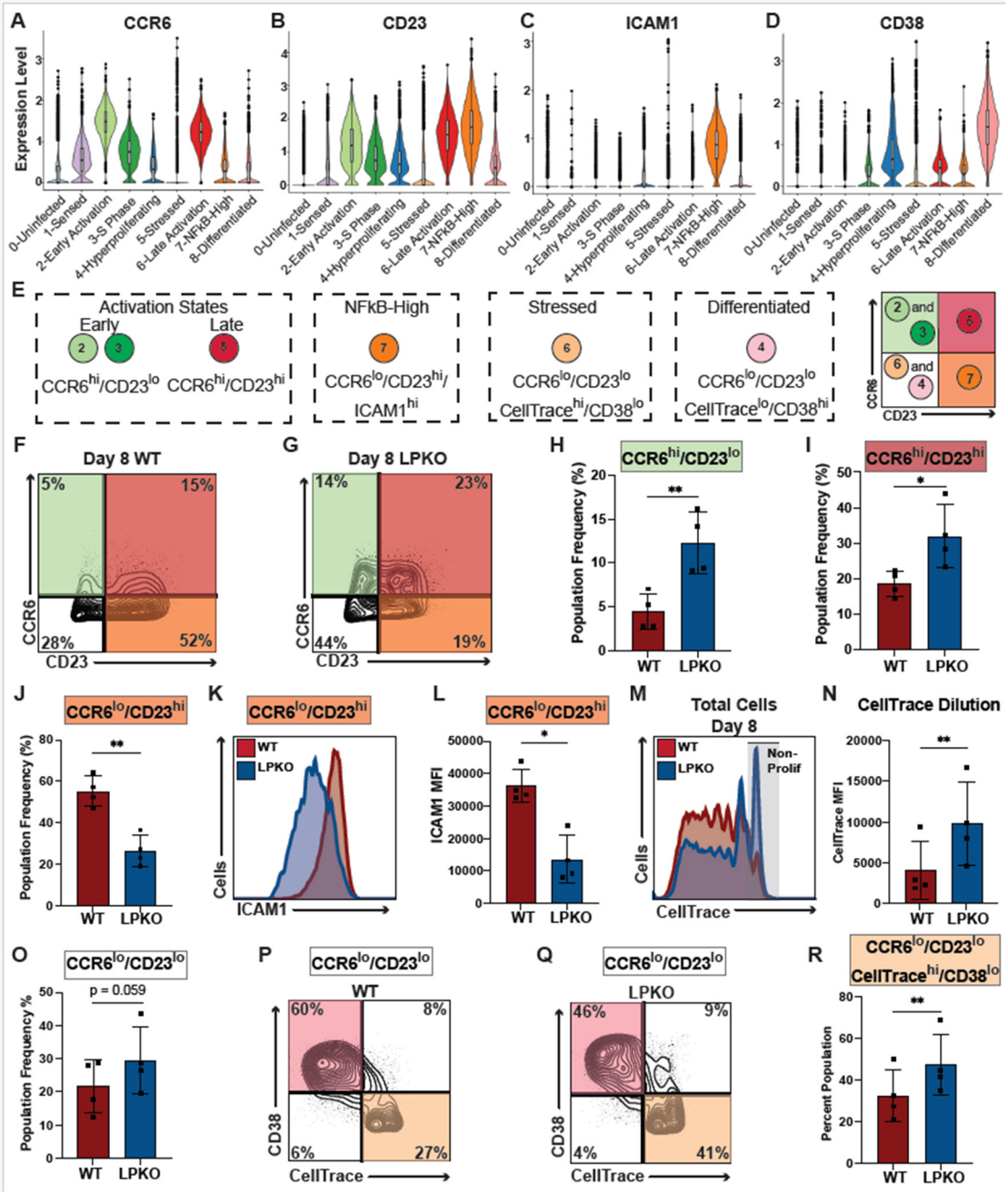

Fig. 2. Altered cell populations between WT- and LPKO-infected B cells identified in scRNAseq data are validated by flow cytometry 8 days post-infection. Expression levels of

CCR6 (**A**), CD23 (**B**), ICAM1 (**C**), and CD38 (**D**) in scRNA-seq clusters. (**E**) Legend of flow panel marks for the key states identified. Flow staining for CCR6 and CD23 8 days post-infection in representative Donor 2 for WT (**F**) and LPKO (**G**) infected B cells. Quadrant color corresponds to cell states that can be distinguished as depicted in (**E**). Percent of WT- and LPKO- infected cells 8 days post-infection in the CCR6^{hi}/CD23^{lo} (Early Activation) states (**H**), the CCR6^{hi}/CD23^{hi} (Late Activation) state (**I**), and the CCR6^{lo}/CD23^{hi} (NFκB-High) states (**J**). (**K**) Histogram comparing expression of ICAM1 protein (proxy for LMP1) between WT and LPKO infected cells in CCR6^{lo}/CD23^{hi} population. (**L**) Quantified Median Fluorescence Intensity (MFI) of ICAM1 signal in CCR6^{lo}/CD23^{hi} population in WT and LPKO infections (n = 4). (**M**) Histogram of CellTrace stain, diluted during each cell division, 8 days post infection in WT and LPKO infected cells in representative Donor 1. Grey area indicates cells that have not proliferated. (**N**) MFI of CellTrace (n=4). Lower MFI indicates more cell proliferation. (**O**) Percent of WT and LPKO infected cells 8 days post-infection in the CCR6^{lo}/CD23^{lo} states (n=4). Separation of CCR6^{lo}/CD23^{lo} populations in WT (**P**) and LPKO (**Q**) infection by CD38 and CellTrace to distinguish Differentiated cells from Stressed cells. (**R**) Percent of CCR6^{lo}/CD23^{lo} cells that are also CD38^{lo} and CellTrace^{hi} (indicating low proliferation) representing the stressed cell cluster. Significance determined with ratio paired t test. N = 4 biological replicates. *Indicates p value less than or equal to 0.05, ** indicates p value less than or equal to 0.01. Histograms are scaled as percent of maximum count (modal).

Using Flow cytometry to analyze protein expression of identified markers in a new set of infected samples, we classified cells by CCR6 and CD23 levels (**Fig. 2F, 2G, S3A, and S3B**) and confirmed the prolonged presence of LPKO-infected cells in states of early activation (c2 and c3) (CCR6^{hi}/CD23^{lo}) (**Fig. 2H**) and late activation (c6) (CCR6^{hi}/CD23^{hi}) (**Fig. 2I**) compared to WT infection. Second, we confirmed that LPKO-infected cells have reduced transition to NFκB-high state (c7), as LPKO-infected cells have reduced CCR6^{lo}/CD23^{lo} populations (**Fig. 2J)** and the cells that do enter this state express significantly less ICAM1 **(Fig. 2K, 2L, and S3C)** compared to WT. Furthermore, compared to WT, LPKO-infected cells are less proliferative (**Fig. 2M, 2N, and S3D).** And, upon further separating CCR6^{lo}/CD23^{lo} cells based on CD38 expression and proliferation, we confirmed that compared to WT, LPKO-infected cells are more frequently in states of cellular stress (c5) (CCR6^{lo}/CD23^{lo}/CellTrace^{hi}/CD38^{lo}) (**Fig. 2O-2R, S3E, and S3F**). Altogether, these data support a model in which EBNA-LP is important in preventing the arrest, stress response, and immune activation after EBV infection.

LPKO-Infected Cells Fail to Suppress the Antiviral Response and Fail to Induce Cellular Metabolic Remodeling

We next sought to characterize the molecular mechanisms underlying the cell fate restrictions following LPKO infection. We first pooled all time points for each WT and LPKO scRNAseq dataset into a “pseudo-bulk” dataset and performed gene set enrichment analysis (GSEA) to identify differentially regulated pathways between WT and LPKO infection. In WT-infected cells, we observed significant enrichment of transcripts involved in NFκB signaling (**Fig. 3A**) in agreement with the failure of LPKO-infected cells to generate an NFκB-high state (**Fig. 1L**). We also observed an increase in expression of genes controlling cellular metabolism in WT- relative

to LPKO-infected cells (**Fig. 3A**). In contrast, LPKO-infected cells were enriched for transcripts of interferon-stimulated genes (ISGs) and antiviral responses (**Fig. 3B**).

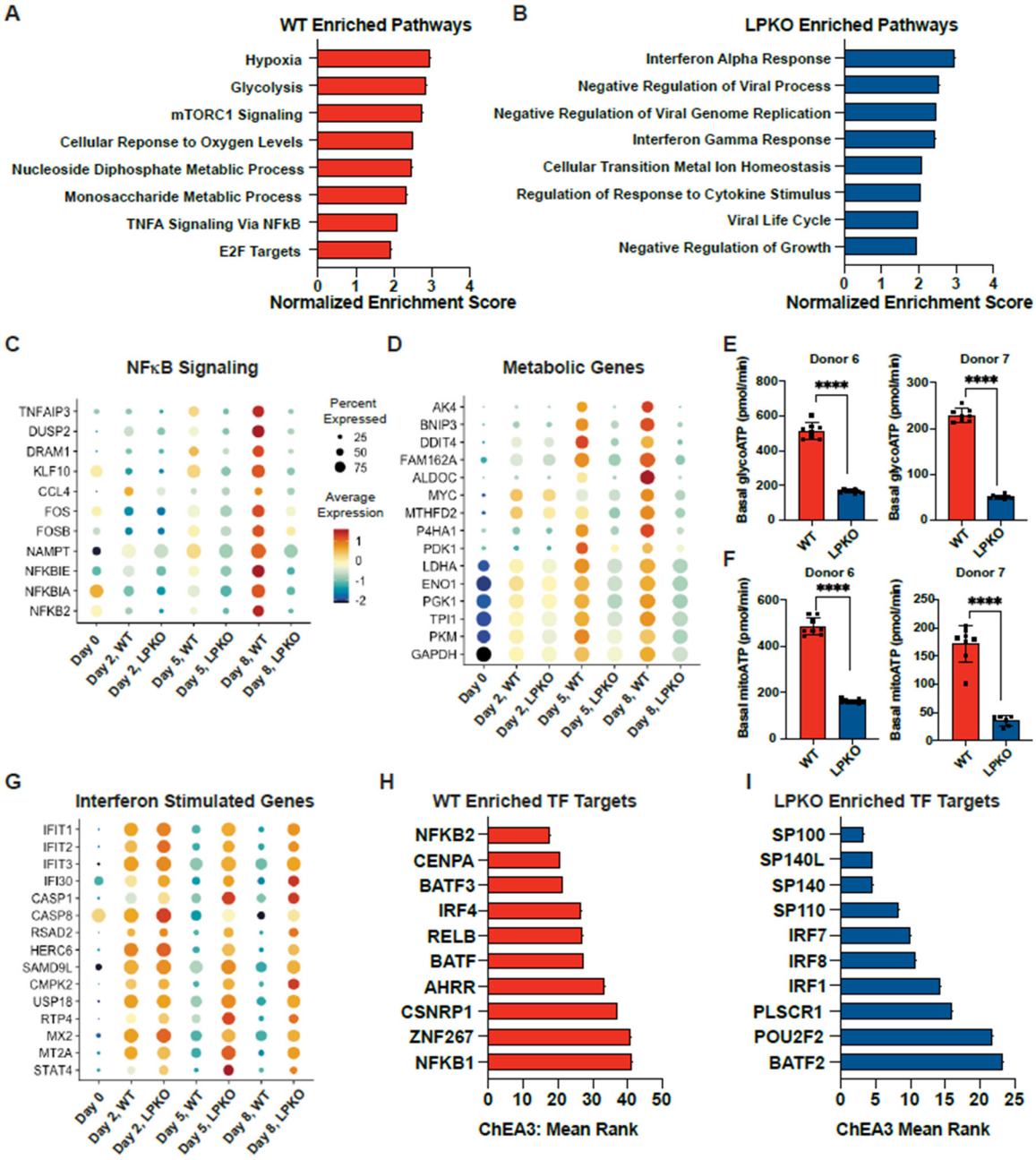

Fig. 3. EBNA-LP promotes expression of pro-proliferative genes, while reducing expression of anti-viral genes. Pathways identified as enriched in WT- compared to LPKO- (**A**) or LPKO- compared to WT- (**B**) infected scRNAseq samples by GSEA Hallmark gene sets or Gene Ontology datasets. Representative top-ranking pathways with false discover rates (FDR q-values) less than 0.05. Higher normalized enrichment score indicates stronger enrichment. Dot plot of representative NFκB signaling-related genes (**C**) and metabolism genes (**D**) identified in GSEA pathways enriched in WT infected cells for each sample in the scRNAseq time course. (**E**) Basal rate of ATP derived from glycolysis (glycoATP) in WT- and LPKO-infected naïve B cells 4 days post-infection in two donors. (**F**) Basal rate of ATP derived from oxidative phosphorylation (mitoATP) in WT- and LPKO-infected naïve B cells 4 days post-infection in two donors. (**G**) Dot plot of representative Interferon

Stimulated Genes enriched in LPKO-infected cells for each sample in the time course. (**H**) Top ten predicted transcription factors identified by ChEA3 associated with expression of the genes enriched in WT-infected cells in scRNAseq samples compared to LPKO or (**I**) LPKO-infected cells compared to WT. Lower mean rank indicates a stronger correlation.

We next used time-resolved pseudo-bulk analysis to better define the dynamic nature of EBNA-LP-dependent gene regulation. NFκB targets were modestly decreased 2 days post-infection in both WT and LPKO-infected cells, but then diverged at 5, and more so at 8, days post infection (**Fig. 3C**). Cellular metabolic gene expression diverged by day 5, following the first EBV-induced cell division (**Fig. 3D**). While loss of NFκB signaling is concurrent with failure to efficiently express LMP1 (44) (**Fig. S2U**), failure to upregulate cellular metabolism in the absence of EBNA-LP was previously unexplored. Therefore, we further examined cellular metabolic activity during early infection and confirmed naïve B cells infected with LPKO virus had reductions in both basal glycolysis and oxidative phosphorylation compared to WT infected cells at 4 days post-infection (**Fig. 3E and 3F**).

Transcripts downregulated upon expression of EBNA-LP (i.e. induced in LPKO-infected cells) were primarily ISGs. Intriguingly, though, interferon gene mRNAs were not elevated in LPKO-infected cells (**Fig. S4A**), indicating ISG induction may occur through other mechanisms. These ISG transcripts are widely induced by two days post-infection in both WT- and LPKO-infected cells (**Fig. 3G**). In the presence of EBNA-LP, WT-infected cells effectively down-regulated expression of these ISGs, whereas in LPKO-infected cells, levels of these ISG transcripts were sustained or increased (**Fig. 3G**). These trends in differentially expressed pathways observed in the scRNAseq data were confirmed by bulk RNAseq of WT- and LPKO-infected cells in additional donors at 8 days post-infection (**Fig. S4B-S4F**).

Because the ISG induction appeared to be independent of IFN induction, we sought to identify which cellular factors could be mediating the observed gene expression differences in WT- and LPKO-infected cells. We used ChEA3 (61) (ChIP-X Enrichment Analysis Version 3) to identify transcription factors whose target genes were enriched in the transcriptome of WT- and LPKO-infected cells. Genes upregulated in WT-infected cells were associated with factors including NFκB subunits; CENPA – a centromere protein and transcriptional regulator that forms a complex with YY1 (62) which we recently identified as an EBNA-LP-interacting protein (53); and IRF4, which can suppress ISG transcription (63), induce expression of Myc (63, 64), and function in cooperation with BATF and BATF3 that are also suggested mediators of these expression changes by the analysis (65, 66) (**Fig. 3H**). Genes upregulated in the absence of EBNA-LP were instead associated with all four human speckled proteins (Sp100, Sp110, Sp140, and Sp140L) (**Fig. 3I**).

Sp100 and Sp140L, but Not Other PML-NB Proteins, are Required to Restrict EBV Transformation in the Absence of EBNA-LP

To examine whether the ChEA3-identified speckled proteins or other PML-NB proteins specifically restrict EBV infection in the absence of EBNA-LP, we assessed the effect of knocking out these target genes on rescuing the inability of LPKO virus to transform naïve B cells. Naïve B cells isolated from adult peripheral blood (**Fig. S5A**) were directly transfected with Cas9-guide RNA ribonucleoprotein (Cas9/RNP) complexes targeting genes encoding the main components of PML bodies, including the speckled proteins, along with CD46, a non-essential cell surface protein used as a proxy for knockout of the target gene (67) (**Fig. 4A**). Transfected cells were then infected with either the LPKO or WT virus, and outgrowth of edited, CD46-negative cells was assessed by flow cytometry weekly post-infection, for 4 weeks (**Fig. 4A**). As expected, control LPKO-infected cells in which only *CD46* was targeted failed to sustain proliferation to generate LCLs, whereas WT EBV still transformed the naïve B cells into LCLs (**Fig. 4B-4D**). While knockout of most of the PML-NB-associated proteins that were targeted – including *PML* – had no significant impact on the outgrowth of LPKO-infected cells, which decreased in number over time like the *CD46*-only knockout, mutation of either *SP100* or – even more emphatically – *SP140L* rescued outgrowth (**Fig. 4B and 4C**). Indeed, knockout of *SP100* or *SP140L* was sufficient to consistently generate LPKO LCLs by 28 days post-infection (**Fig. 4D**) and target genes were efficiently knocked out in these LCLs as validated by genomic DNA sequencing (**Fig. S5B**) and protein expression where applicable (**Fig. S5C**). Additional LPKO LCLs were generated after a longer time in culture with inconsistent target knockout (**Fig. S5D**), likely arising from contaminating memory B cells. Targeting the same factors in WT infected cells had no impact on outgrowth (**Fig. S5E and S5F**), confirming Sp100 and Sp140L restrict EBV infection only in the absence of EBNA-LP.

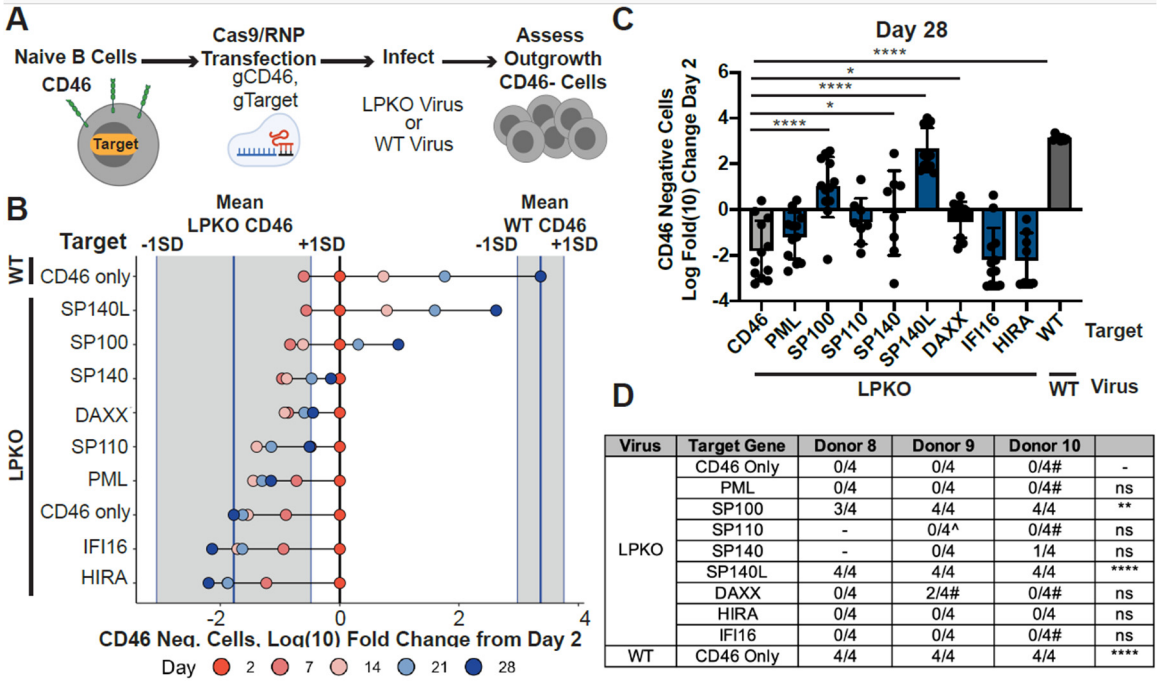

D

Virus	Target Gene	Donor 8	Donor 9	Donor 10	
LPKO	CD46 Only	0/4	0/4	0/4#	-
	PML	0/4	0/4	0/4#	ns
	SP100	3/4	4/4	4/4	**
	SP110	-	0/4^	0/4#	ns
	SP140	-	0/4	1/4	ns
	SP140L	4/4	4/4	4/4	****
	DAXX	0/4	2/4#	0/4#	ns
	HIRA	0/4	0/4	0/4	ns
	IFI16	0/4	0/4	0/4#	ns
WT	CD46 Only	4/4	4/4	4/4	****

Fig. 4. Knockout of *SP140L* or *SP100* rescues transformation of LPKO-infected naïve B cells. (**A**) Schematic of Cas9/RNP screening approach. (**B**) Log(10) Fold Change from Day 2 of the total number of CD46 negative cells for each condition 2, 7-, 14-, 21-, and 28-days post-infection. Dark turquoise line represents the mean number of CD46 negative cells in CD46 only control WT- or LPKO- infected cells 28 days post infection. SD = standard deviation. (**C**) Total number of CD46 negative cells 28 days post infection for each condition plotted as log fold change from 2 days post infection. P values calculated by one-way ANOVA with multiple comparisons to compare to LPKO infected cells transfected with guide targeting CD46 only as control. *Indicates p-values <0.05, ** indicates p-values <0.01, **** indicates p value < 0.0001. (**D**) Total number of LPKO LCLs in each donor for each target out of 4 replicates per donor. #Indicates conditions in which at least one LCL was generated after an additional three weeks in culture with variable knockout efficiency. ^Indicates conditions in which at least one LCL was generated in the same time frame at WT virus, but target gene was not knocked out. P values calculated using Fischer's exact test to compare outcomes to LPKO control condition ** indicates p-values <0.01, **** indicates p value < 0.0001.

Structural characterization of EBNA-LP/Sp140L and Sp100 interactions define a critical interface important for B cell transformation

To better understand the nature of the putative interaction between EBNA-LP and Sp140L and Sp100, we used Alphafold3 to predict the structure of a complex between these proteins (68). First, we found that despite EBNA-LP being predicted to have high intrinsic disorder (45), AlphaFold3 consistently predicted that EBNA-LP forms an extended beta sheet, with loops connecting helices derived from the repeated W domains and a loop extending the unique 45 amino acid Y domain containing a short alpha helix (**Fig. 5A and 5B**). The interaction sites with Sp140L and Sp100 are consistently predicted to involve this Y domain alpha helix engaging a CARD domain derived helical bundle of Sp140L and Sp100 (**Fig. 5C and 5D**), the latter being consistent with prior biochemical findings (38). Specifically, the hydrophobic interface of these interactions relies on a conserved leucine rich motif (LRM) within EBNA-LP (53) (**Fig. 5E and 5F**). Indeed, modification of

the leucines in this helix to alanines was sufficient to disrupt the association between EBNA-LP and Sp100 by co-immunoprecipitation (**Fig. 5G**).

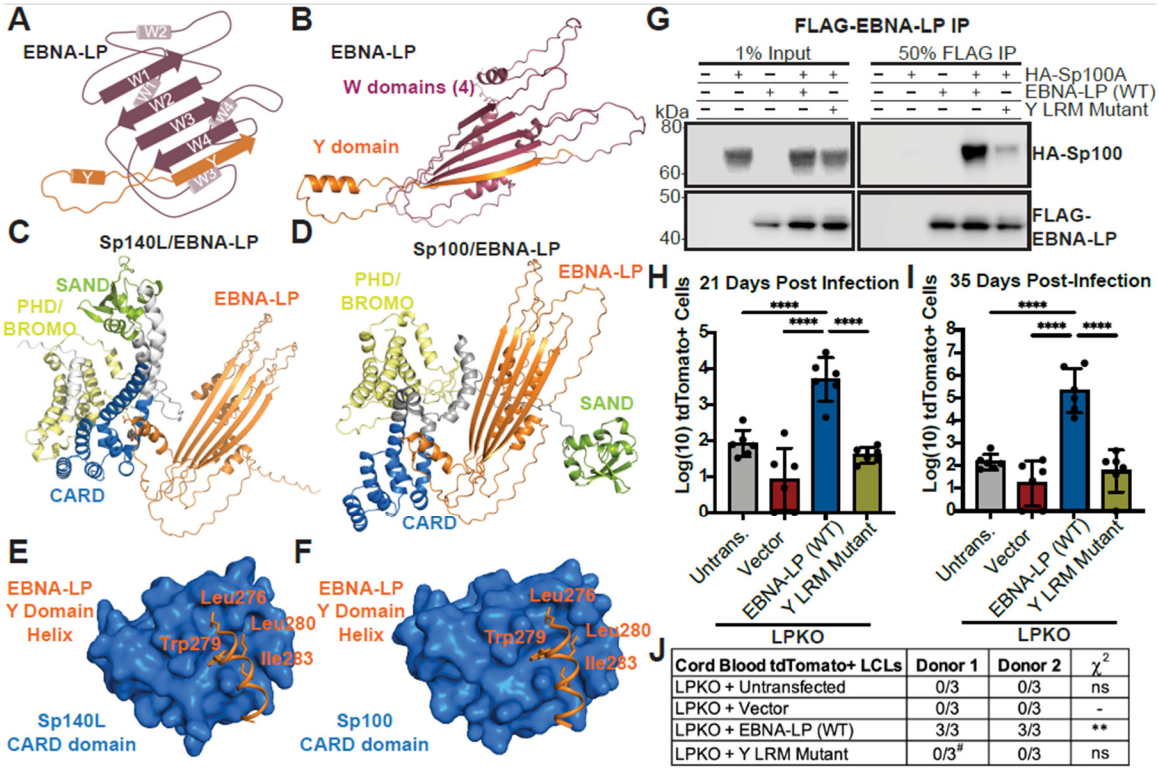

J

Cord Blood tdTomato+ LCLs	Donor 1	Donor 2	χ^2
LPKO + Untransfected	0/3	0/3	ns
LPKO + Vector	0/3	0/3	-
LPKO + EBNA-LP (WT)	3/3	3/3	**
LPKO + Y LRM Mutant	0/3#	0/3	ns

Fig. 5. EBNA-LP is predicted to engage Sp140L and Sp100 through an alpha-helix containing a leucine-rich motif in the C-terminal Y domain. (**A**) Schematic of EBNA-LP (encoding 4 repeated W domains) predicted structure W (magenta) and Y domain (orange) contributions to beta strands and alpha helices based on **B**. (**B**) Alphafold3-predicted model of EBNA-LP three-dimensional structure. Predicted model of EBNA-LP (orange) in complex with (**C**) Sp140L and (**D**) in complex with Sp100. Speckled protein domains are highlighted: CARD domain (blue), SAND domain (green), PHD/BROMO domain (yellow). Zoomed in view of EBNA-LP Y domain helix (spanning amino acids 276 through 287) encoding the leucine-rich motif in contact with (**E**) Sp140L and (**F**) Sp100 CARD domains. EBNA-LP residues with side-chains predicted to contact CARD domains are indicated. **G**. FLAG co-immunoprecipitation of FLAG-tagged EBNA-LP wild type or mutant with leucines in Y domain alpha-helix modified to alanine (Y LRM Mutant, L276,280,281A) with HA-Sp100 Isoform A performed in 293T cells. EBNA-LP constructs encode 4 W domains. 1% of input material and 25% of co-immunoprecipitation was used for imaging. (**H**)Total tdTomato positive cells in each condition of cord blood B cells infected with LPKO and trans-complemented with indicated DNA construct 21 days post-infection and (**I**) 35 days post-infection (performed in two donors, with 3 replicates each). Untransfected cells indicates background signal threshold. P values calculated by ordinary one-way ANOVA with Dunnett's multiple comparisons test. **** Indicates p value < 0.0001. (**J**) Number of tdTomato positive LCLs generated per condition. # Indicates a single replicate in which cells were transformed but were not tdTomato positive. P values were calculated using Fisher's exact test to compare transformation outcomes to LPKO-infected cells trans-complemented with empty vector. ** Indicates p value < 0.01.

To further examine the role of the Y domain LRM at the speckled protein interface in transformation of naïve B cells, we used a trans-complementation assay in cord blood B cells infected with LPKO virus as previously described (53). Prior to infection, cells were transfected with an episomal plasmid encoding tdTomato and either wild type or an EBNA-LP mutant in which

393 leucines were mutated to alanine. We first confirmed expression of the mutant protein in LPKO-
394 transformed total B cells, since EBNA-LP is not required for the transformation of the memory B
395 cell component, and demonstrated that both wild type and mutant EBNA-LP are able to be
396 expressed (**Fig. S6A**) and had the same sub-cellular localization profile as EBNA-LP expressed
397 from WT virus (**Fig. S6B**). EBNA-LP with a mutated Y domain LRM failed to rescue transformation
398 of LPKO-infected cord blood B cells compared to wild-type EBNA-LP (**Fig. 5H – 5J**) – indicating
399 that the Y domain LRM of EBNA-LP involved in Sp100 and likely Sp140L interaction is essential
400 during EBV infection.
401
402
403 ***SP100* or *SP140L* Knockout Rescues Cellular and Viral Gene Expression Critical for Naïve**
404 **B Cell Outgrowth**
405 We then sought to investigate the mechanism by which Sp100 and Sp140L restrict EBV
406 infection in the absence of EBNA-LP. We used bulk RNAseq to examine the effect of *SP100* and
407 *SP140L* knockout on viral and cellular gene expression five days after LPKO infection of naïve B
408 cells (**Fig. S7A**). Knockout of *SP100* or especially *SP140L* reduced induction of IFN-related genes
409 in LPKO-infected cells (**Fig. 6A-6D**). Knockout of either *SP100* or *SP140L* also rescued the
410 expression of pathways important for proliferation including MYC targets, E2F targets, and
411 particularly upon *SP140L* knockout, metabolic pathways (**Fig. 6A-6C and 6E**). NFκB signaling was
412 also rescued by *SP100* and *SP140L* knockout in LPKO infected cells (**Fig. 6A-6C and 6F**), with
413 knockout of *SP140L* again exhibiting in a more complete rescue of gene expression towards wild-
414 type levels – in agreement with the transformation screen (**Fig. 4B**). Since LMP1 and other viral
415 genes are inefficiently activated during LPKO infection (44), we examined viral latency gene
416 expression, and found that *LMP1* and *LMP2* RNA levels in LPKO infected cells were somewhat
417 elevated upon loss of *SP100* and largely recovered in *SP140L* knockouts (**Fig. 6G**). This was
418 further confirmed at a functional level by flow cytometry using ICAM1 as a proxy for LMP1, as
419 knockout of *SP100* or – to a greater extent – *SP140L* rescued surface ICAM1 protein to levels
420 comparable to WT infected cells (**Fig. 6H and S7B**).

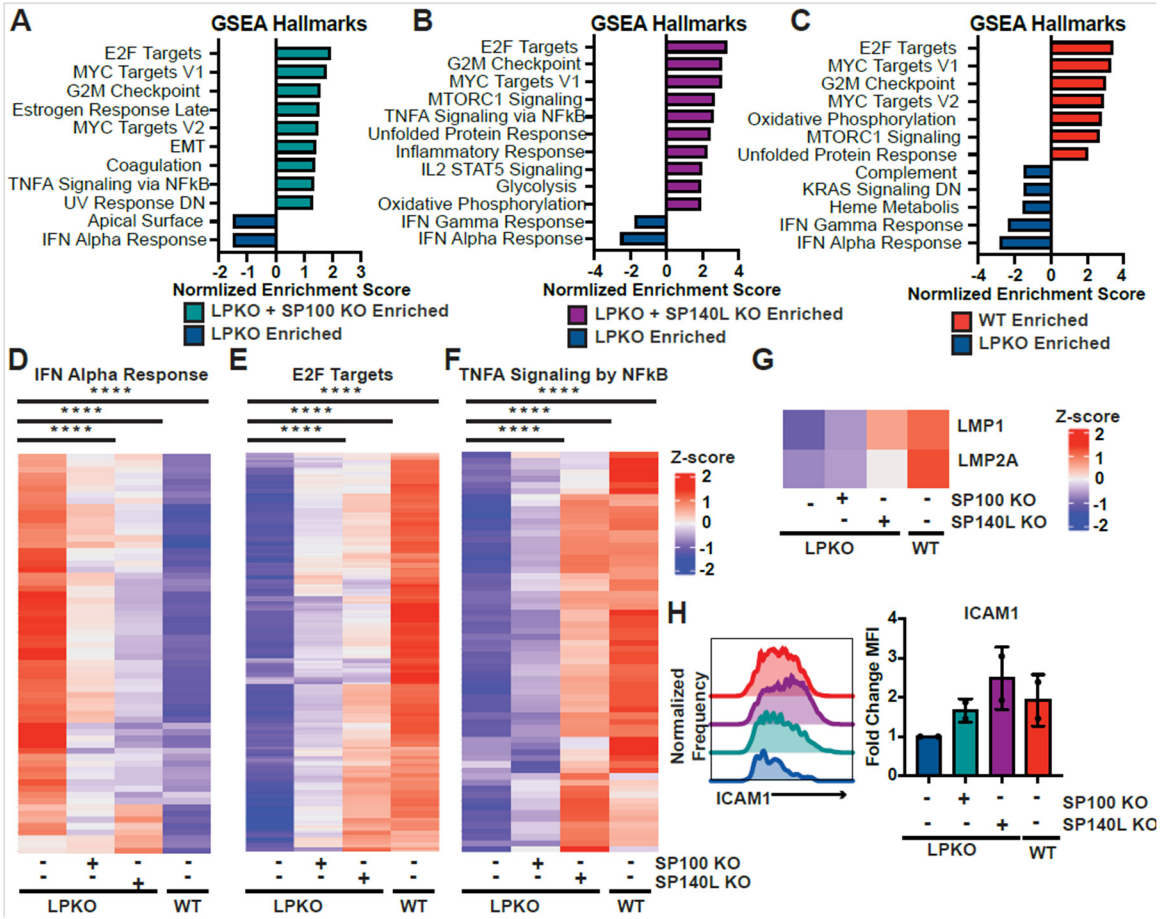

Fig. 6. *SP100* and *SP140L* Knockout in LPKO-infected cells promotes transcription of pathways required for outgrowth and inhibits the anti-viral response. GSEA Hallmark pathway analysis of bulk RNA-sequencing samples 5 days post-infection comparing LPKO infected cells with (**A**) *SP100* knockout, (**B**) *SP140L* knockout or WT virus infection (**C**) to in comparison control LPKO infection (n = 2). GSEA terms with nominal p value less than 0.05 are shown. Higher absolute value of the normalized enrichment score indicates stronger enrichment. Heatmap of genes related to the significantly enriched Hallmark pathways (**D**) "Interferon (IFN) Alpha Response," (**E**) "E2F Targets", and (**F**) "TNFA Signaling by NFκB" for each condition. Average z-score of two samples is plotted. P values determined by One-way Repeated Measures ANOVA with multiple comparisons to LPKO control. **** indicates p value less than 0.0001. (**G**). Average Z-score for mRNA encoding LMP1 and LMP2A for each sample. (**H**)**.** Histogram of flow cytometry signal for LMP1 proxy gene ICAM1 in each sample.

Sp140L Also Restricts ORF3-Deficient Herpesvirus Saimiri (HVS)

As Sp140L has not previously been studied as a viral restriction factor, we sought to determine whether Sp140L can restrict herpesviruses other than EBV, and in cell types other than B cells, by studying Sp140L in HVS infection. As the HVS tegument protein ORF3 targets Sp100 for degradation(34), we generated two independent WT HVS and ORF3-KO HVS viruses (**Fig. S8A and 8B**) carrying a CMV promoter-driven luciferase expression cassette. We confirmed infection of human fibroblast HFF cells with WT HVS, but not ORF3-KO HVS, resulted loss of Sp100 protein (**Fig. S8C**). We then compared virus transcription after initial infection in two human fibroblast cell

443 lines (HFF and MRC5 cells) carrying knockout of either *SP100* or *SP140L* alongside the proxy gene
444 *CD46* (**Fig. 7A**). Consistent with a previous report with an ORF3-KO of a C-strain HVS (34),
445 knockout of *SP100* rescued viral transcription after ORF3-KO HVS infection (**Fig. 7B and 7C**).
446 Consistent with our EBV data, knockout of *SP140L* was also sufficient to rescue luciferase
447 expression from the ORF3-KO virus in both cell types (**Fig. 7B and 7C**). Loss of *SP100* or *SP140L*
448 in the context of WT HVS infection had little or no effect on viral transcription (**Fig. S8D-S8F**)
449 suggesting that ORF3 antagonizes both Sp100 and Sp140L function during WT HVS infection.
450 These findings suggest Sp140L is a restriction factor of diverse gammaherpesviruses in primates,
451 that is at least as important as Sp100.

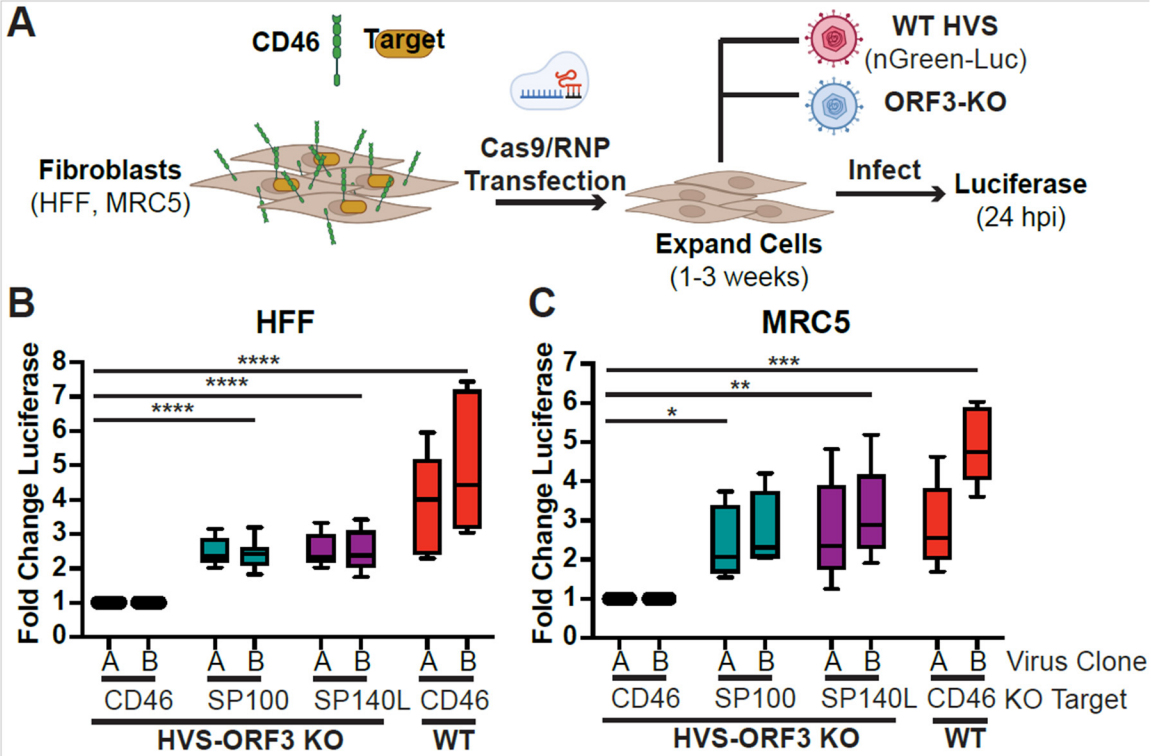

452
453 **Fig. 7. Sp100 and Sp140L restrict Herpesvirus Saimiri (HVS) in the absence of ORF3.** (**A**).
454 Schematic of experiment. Fold change in luciferase expression HFF cells (n=7) (**B**) or MRC5 cells
455 (n=5) (**C**) infected with HVS-ORF3 Knockout or WT virus encoding luciferase with knockout of
456 control *CD46*, *SP100*, or *SP140L*. Two virus preparation (A and B) were used. P values calculated
457 by Dunnett's multiple comparisons test using an ordinary two-way ANOVA. * Indicates p-values
458 <0.05, ** indicates p-values <0.01, **** indicates p value < 0.0001.
459
460 **Discussion**

461 Herpesviruses infect nearly all animal species and result in lifelong latent and persistent
462 infections (69). As DNA viruses, herpesviruses must overcome cellular barriers to establish
463 infection, including the detection and chromatinization of their foreign DNA genomes by intrinsic
464 restriction factors such as those in PML-NBs, including Sp100. Here, we have identified Sp140L,
465 an Sp100-homolog, as a novel restriction factor of herpesvirus infection that is counteracted by the
466 EBV latency protein EBNA-LP and the HVS tegument protein ORF3. Our data are consistent with

467 a mechanistic model whereby both Sp100 and Sp140L restrict EBV infection by preventing the
468 expression of the essential viral latency genes that are expressed after EBNA-LP and EBNA2, and
469 by altering cellular gene expression - both inducing an ISG response and reducing B cell metabolic
470 capacity. While the core antiviral PML-NB proteins have been thought to include PML, Sp100,
471 DAXX, and ATRX, our work adds the evolutionarily recent Sp140L to the list of key cellular intrinsic
472 restriction factors of DNA viruses in primates.

473 Leveraging a targeted CRISPR screen, we identified Sp100 and Sp140L as key restriction
474 factors that prevent EBV transformation of naïve B cells in the absence of EBNA-LP and viral
475 transcription of HVS in the absence of ORF3. Since knocking out other PML-NB components did
476 not rescue LPKO EBV, these other components of PML-NBs must either be fully targeted by other
477 EBV proteins, exhibit functional redundancy, or are not required to block EBV-mediated
478 transformation. Based on studies of HSV and CMV mutants that lack abilities to inhibit PML-NB
479 functions (13, 30, 32, 70, 71), we can conclude that PML-NBs have two parallel repressive
480 pathways in humans: one driven by DAXX/ATRX and another by Sp100 and – we now propose –
481 Sp140L. In the LPKO virus, its DAXX-counteracting tegument protein BNRF1 is still intact,
482 suggesting that factors in our screen that failed to rescue naïve B cell transformation may be part
483 of the DAXX-associated pathway. While DAXX/ATRX load repressive histones (e.g. H3.3) onto the
484 incoming viral genome (13), Sp100 and Sp140L may be responsible for the addition of repressive
485 histone marks such as H3K9me3 and/or H3K27me3. For example, during latent KSHV infection of
486 endothelial cells, loss of Sp100, but not DAXX nor PML, correlates with H3K27me3 deposition on
487 the viral genome (72), although Sp100's ability to bind heterochromatin protein 1 (HP1) and high-
488 mobility group protein B1 (HMGB2) (73) suggests Sp100 may also be linked to H3K9me3 (74).

489 While PML-NB components are known to restrict DNA virus gene expression, we
490 discovered that Sp100 and Sp140L are also important in suppressing cellular proliferation. Possible
491 mechanisms of restricting proliferation include the failure to express the LMPs during LPKO
492 infection, however, LMP1 is not essential for the initial cell divisions after EBV infection (75). An
493 alternative mechanism explaining these results is that these factors integrate intrinsic DNA sensing
494 with an anti-proliferative ISG response. Recent evidence suggests Sp100 can localize to ISG
495 promoters (10) suggesting Sp100 – and perhaps by extension Sp140L – induce ISGs through direct
496 transcriptional regulation or chromatin modification at ISG promoters - as has been observed with
497 other PML-NB components including HIRA (7, 8), ATRX(9), and PML (11) in mutant HSV- and
498 HCMV-infected cells or upon IFN stimulation. We also observed a restoration of expression of
499 proliferation-linked genes upon knockout of *SP100* or – more convincingly – *SP140L*, suggesting
500 that detection of foreign DNA or upregulation of ISG proteins may repress pro-proliferative genes.
501 For example, RSAD2, an ISG highly expressed during LPKO compared to WT EBV infection,
502 influences cellular metabolism and mitochondrial function (76, 77). IRF proteins can also target
503 metabolic genes (78, 79), and notably several IRFs were also identified as potential mediators of

504 gene changes in LPKO-infected cells by ChEA3 (**Fig. 3G and 3H**). In contrast, whether Sp100 and
505 Sp140L impose cellular arrest by functioning as cell cycle checkpoint proteins, therefore resulting
506 in loss of proliferation-associated genes remains unknown. Still, these findings suggest Sp100 and
507 Sp140L impose an antiviral state through not only regulating key viral genes, but also through
508 repression of cell cycle progression to impose an anti-proliferative state not favorable for viral
509 infection or transformation.

510 To further investigate the mechanism by which EBNA-LP may disrupt Sp100 and Sp140L,
511 we used AlphaFold3 to generate the first predicted structure of EBNA-LP and found that an alpha
512 helix in the C-terminal Y domain of EBNA-LP is predicted to associate with the CARD domain of
513 Sp100 and Sp140L. Mutagenesis of the leucine-rich motif (LXXXLL) within this alpha helix disrupts
514 EBNA-LP's interaction with Sp100 and likely Sp140L, and reduces the ability of EBNA-LP to trans-
515 complement the LPKO virus in the transformation of naïve B cells. Our previous work identified this
516 motif as important for EBNA-LP to associate with the cellular transcription factor YY1 (53). This
517 motif is similar in sequence to both the LXXLL motif found in many cellular proteins that regulate
518 transcription (80), and to a similar but more diverse in sequence motif termed "flexiNR" that is
519 encoded in many viral proteins with transcription regulation functions (81). Our findings fit with the
520 notion that many viral proteins, including viral oncoproteins, have evolved short linear motifs,
521 generally less than 10 residues long in which a few key residues define affinity and specificity, in
522 order to mimic and/or hijack cellular protein functions (82, 83). One such example includes the
523 LXCXE motif in the many viral proteins that can promote S Phase transition through interaction with
524 pRb, p107, and p130 (84). Therefore, this LXXXLL motif is an example of short linear motif critical
525 for viral protein function.

526 This study was strengthened by the use of primary cells rather than cancer cell lines. This
527 is critical as PML-NBs functions can be disrupted in cancer cells, and therefore the use of cancer
528 cell lines for DNA sensing or virus restriction assay may not reflect physiological relevance (8). Still,
529 there are limitations to performing knockouts in primary B cells, as to reduce cell death prior to
530 infection, B cells are infected with EBV only 2 hours post-transfection. Therefore, as EBNA-LP is
531 one of the earliest expressed EBV latency proteins, turnover of targeted protein may be incomplete
532 by the time EBNA-LP would be expressed, even if genomic editing has occurred, and therefore this
533 assay cannot fully complement the LPKO virus. While the HVS assay using primary fibroblasts to
534 generate knockout cell lines prior to infection does not have the same temporal disadvantage, it
535 was challenging to get complete knockout of target genes even in cells with the proxy target, CD46,
536 lost. While overcoming these limitation would likely allow for an even more pronounced rescue of
537 the LPKO and ORF3-KO viruses with knockout of *SP100* and *SP140L*, our assays clearly show
538 that both *SP100* and *SP140L* restrict these diverse herpesviruses. Furthermore, in our assays,
539 knockout of *SP140L* resulted in stronger phenotypic rescue – supporting Sp140L as the

540 predominant speckled protein restricting DNA viruses. However, we cannot exclude the possibility
541 these observations are a result of differences in knockout efficiency between *SP100* and *SP140L*.
542 The *SP140L* gene was formed by a gene duplication and cross-over event between *SP100*
543 and *SP140* shortly prior to the emergence of primates (29). As a result, the Sp140L N-terminal
544 CARD domain is over 90% identical to that of Sp100, while its C-terminal SAND and
545 PHD/Bromodomains are very like those of Sp140 (29). Sp140L also lacks the exons that in Sp100
546 encode SUMOylation and HP1 binding motifs but retains the exons that in Sp100 can bind to the
547 high mobility group protein HMGB2. Given the CARD domain is responsible for the dimerization(24,
548 85) or multimerization(86) of Sp100 and that Sp100 and Sp140L colocalize in cells (29), and that
549 Sp100 can form homotypic interactions with the more distantly related protein Sp110 (87), we
550 anticipate that Sp100 and Sp140L can interact, perhaps interchangeably, through this domain. This
551 is further supported by our findings that knockout of either Sp100 or Sp140L alone was sufficient
552 for rescue of transformation. Whether Sp140L arose as the result of an evolutionary arms race with
553 viral antagonists of Sp100 remains a possibility. As knockout of Sp140 did not enhance
554 transformation of either WT- or LPKO-infected B cells, further analysis of the molecular differences
555 between Sp140L and Sp140 – and the key domains responsible for DNA virus restriction requires
556 further investigation. Additionally, expression differences between Sp100 and Sp140L may
557 contribute to the dependency of EBNA-LP in naïve, but not memory B cell transformation as at the
558 RNA level, naïve B cells more highly express both Sp100 and Sp140L (88).
559 Based on what is known about Sp100, we can propose the following model for how both
560 Sp100 and Sp140L might sense and suppress incoming viral genomes. The SAND domain of
561 Sp100 is reported to preferentially bind pairs of unmethylated CpG dinucleotides (89). Its
562 PHD/Bromodomain contains bulky residues where other PHD/Bromodomains contain binding
563 pockets for histone modifications (90). CARD domains commonly multimerize through homotypic
564 interactions to activate immune signaling pathways (91). Speckled proteins Sp100, Sp110 (87),
565 and Sp140 (92, 93) also associate on cellular chromatin at gene promoters including Sp100A at
566 ISGs (10), with Sp140 localizing to sites enriched in H3K27me3 to maintain heterochromatin (92,
567 93). We hypothesize therefore that the SAND domain of Sp100 (and by extension Sp140L)
568 recognize the unmethylated incoming viral DNA as foreign, perhaps in combination with the
569 PHD/Bromodomain recognizing features of newly assembled chromatin. Multimerization of Sp100
570 and Sp140L proteins along the viral genome can then block the initiation of transcription of viral
571 genes (with only immediate early genes having escaped repression) either directly or by recruiting
572 repressors like HP1 or other chromatin remodeling factors to promote or maintain the viral genome
573 heterochromatin. Meanwhile, viral infection may also influence Sp100 and/or Sp140L localization
574 to cellular gene promoters, perhaps relieving repressive epigenetic marks at the loci of ISGs.
575 Alternatively, multimerization of the CARD domains nucleates a signaling process that activates

576 transcription of ISGs (87), activating cell division checkpoints to suppress proliferation of a cell that
577 has potentially been invaded by a persistent foreign genome.
578 In conclusion, we identify Sp140L as a restriction factor of herpesviruses, and likely all DNA
579 viruses, targeted by critical viral proteins of primate viruses, but may represent a significant barrier
580 to any virus with a nuclear DNA phase of its lifecycle that transmits from non-primate mammals.
581 Not only does Sp140L restrict viral infection by preventing the transcription of key viral genes, but
582 also by promoting an ISG response that suppresses cellular pro-proliferative pathways, and curbs
583 the metabolic remodeling required for cellular transformation that is a feature of persistent virus
584 infections.
585
586 **Materials and Methods**
587 **EBV Virus Preparation**

588 WT and LPKO viruses were prepared from 293-EBV producer lines and Raji Green Unit titer was
589 obtained as previously described(44). In brief, LPKO virus refers to LPKO^{w} from Szymula et al.(44)
590 which contains a stop codon in exon W2 of every internal W repeat and WT EBV refers to WT^{w}
591 which contains a repaired stop codon in one W repeat found in the parental B95-8 virus that (unlike
592 B95-8) allows robust EBNA-LP expression (94).

593 **PBMC Isolation and Total/Naïve B and Pan B Cell Enrichment**

594 Adult buffy coats were obtained from the Gulf Coast Regional Blood Center (Pro00006262) and
595 Cord Blood was obtained from the Carolinas Cord Blood Bank (Pro00061264) PBMCs were
596 isolated as previously described (53). Total B cells were isolated using the EasySep Human Pan-
597 B Cell Enrichment kit (STEMCELL Technologies #19554) or MojoSort Human Pan B Isolation kit
598 (Biolegend # 480082). To obtain isolated naïve and memory B cells for SeahorseXF, the EasySep
599 Human Memory B Cell Isolation kit (STEMCELL Technologies #17864) was used. And, to isolate
600 only naïve B cells for the knockout screen and RNA-sequencing, the EasySep Human Naïve B cell
601 isolation kit was used (STEMCELL Technologies, #17254). Purity of isolated cells was assessed
602 by flow cytometry using antibodies to CD19, CD27, and IgD.

603 **EBV Infection**

604 Isolated B cells were infected by adding WT or LPKO virus at a ratio of 0.2 Raji Green Units per
605 cell and incubating at 37°C for 1 hour. Following incubation, cells were pelleted and resuspended
606 in Roswell Park Memorial Institute (RPMI) medium 1640 supplemented with 20% heat-inactivated
607 fetal bovine serum (FBS) (Corning) (R20 media) at approximately 3 million cells/mL.

608 **Collection of scRNAseq samples, library preparation, sequencing, and processing**

609 Samples were viably frozen at each time point in 90% FBS + 10% DMSO and stored in liquid N_2.
610 Cryopreserved samples were then thawed simultaneously and enriched for viable cells by Ficoll
611 gradient. Libraries from 10,000 cells were then prepared in house using the 10x Chromium GEM-
612 X Single Cell 3' Gene Expression kit (10x Genomics,1000691). Libraries were pooled and
613 sequenced by the Duke Sequencing and Genomic Technologies core facility on the NovaSeq 6000
614 S2 at 50 base pair read depth, with paired end reads. Reads were mapped to the human genome
615 and type 1 EBV genome as previously described(54).

616 **scRNAseq QC Filtering and Analysis**

617 scRNAseq analysis was performed in R using package Seurat (95). QC filtering and clustering of
618 samples into subpopulations was performed as previously described(54). To identify the biological
619 features of each cluster, gene ontology analysis was performed using clusterProfiler (96) and the
620 top 100 genes differentially expressed in the previously identified B95-8 subpopulations (54) were
621 compiled and used to add module scores for each subpopulation to the clusters identified in this
622 experiment.

623 **Flow Cytometry**

624 For analysis of B cell isolation purity (CD19, Biolegend, 302212) and CD23 upregulation (Biolegend,
625 338516), naïve B cells isolation purity (IgD Biolgened, 348210, CD27 Biolegend 302824), CD46
626 knockout efficiency (Biolgened, 352405), and ICAM1 expression (Biolegend, 353116) flow
627 cytometry was performed on the BD FACSCanto II (BD Biosciences) and samples were prepared
628 as previously described(53). When quantifying outgrowth of CD46 negative cells, the high
629 throughput sampler was used to collect precise sample volumes.

630 Flow cytometry was also performed to validate the scRNA-sequencing data using the identified
631 markers using spectral flow cytometry on a Cytek Aurora (Cytek Biosciences). Isolated Pan B cells
632 were stained with CellTraceViolet (ThermoFisher, MPK1096) at 0.1 μM in PBS for 20 minutes at
633 37°C with gentle mixing every 5 minutes. Staining was then quenched by adding 4x volume of R20
634 media and incubating for 5 minutes at 37°C. An aliquot of cells was also infected that were not
635 stained with CellTraceViolet to use as a staining control. After pelleting, cells were infected with
636 virus. At each time point collected, cells were first washed in PBS and stained with LiveDead Blue
637 (ThermoFisher, L23105) for 20 minutes in the dark. Samples were then washed with FACS buffer
638 (PBS + 2% FBS) and stained with antibodies as above (CCR6 Invitrogen, 12-1969-42, CD23
639 Biolegend, 338516, ICAM1 Biolegend 353114, CD38 Biolegend 303529). Unstained cells were
640 used for reference controls for unmixing at each time point, along with single stained compensation
641 beads (BD Biosciences, 552843). To ensure accurate staining and analysis, fluorescence minus
642 one controls, isotype controls, and single stained samples were also prepared for each time point.
643 All flow cytometry data was analyzed in FlowJo (FlowJo, LLC).

644 **SeahorseXF Assay**

645 Four days post infection, naïve and memory infected B cells were collected. Using flow cytometry,
646 CD19 and CD23 expression was assessed to ensure comparable infectivity between WT and
647 LPKO.

648 One day prior to the assay, the XFe96 sensor cartridge was submerged in tissue culture grade
649 water overnight at 37°C in a non-CO_2 incubator, along with XF calibrant (Agilent, 100840-00). The
650 following day, the sensor cartridge was then placed in a utility plate containing the pre-warmed XF
651 Calibrant for 1 hour in the non-CO_2 incubator before running the assay.

652 A 96-well Seahorse XF plate was coated with poly-D-lysine to keep suspension cells adhered to
653 the bottom of the wells. Cells were then harvested to the plate at 250,000 cells per well in 50 µL XF
654 Base Medium (RPMI supplemented with 10 mM glucose, 1 mM sodium pyruvate, and 2 mM L-
655 glutamine) (Agilent, 103681-100) and adhered to the plate by briefly centrifugation. 130 µL warm
656 assay media was then added to each well and placed in the non-CO_2, 37°C incubator for 1 hour.

657 The XF Real-time APT Rate Assay was used (Agilent, 103592-100). Ports were loaded with
658 oligomycin and Rotenone/Antimycin A at working concentrations of 1.5 µM and 0.5 µM respectively.
659 The calibrated sensor was then placed in the plate and the assay was then run on the Seahorse
660 XF Pro Analyzer (Agilent).

661 **Bulk RNASeq Sample Collection**

662 RNAseq libraries were prepared from samples 8 days post infection. Pan B cells from three donors
663 total were isolated, however, due to low yield, two of the three donors were pooled together at the
664 time of infection for a total of two Pan B pools infected with separately with WT and LPKO virus. A
665 Ficoll gradient was used to remove dead cells from the harvested samples.

666 RNA-seq libraries were also prepared 5 days post infection for two donors in which naïve B cells
667 were isolated, transfected with guides targeting CD46, CD46 and SP100, or CD46 and SP140L
668 prior to infection with LPKO or WT virus. Due to low cell counts, cells were not sorted and therefore
669 contain a mixed population of CD46 negative and positive cells (**Fig. S6A**), although the majority
670 of cells were CD46 negative.

671 **Bulk RNASeq Library Preparation and Analysis**

672 RNA was isolated using the Qiagen RNeasy mini extraction kit including on-column DNase
673 digestion (74104). Libraries were prepared using the NEBNext Ultra II RNA Library Prep kit (E770S)
674 and sequenced as previously described(53). QC of prepared libraries was assessed using a
675 TapeStation (Agilent). Reads were aligned to hg38 (Day 8 bulk RNAseq samples) or hg38 with the
676 Type 1 EBV genome (Day 5 knockout RNAseq samples) using Hisat2. Samtools was then used to

677 generate bam files. DESeq2 was used to generate a ranked list of differentially expressed genes
678 for Gene Set Enrichment Analysis (GSEA) (97).

679 **Knockout Screen in EBV Infected Naïve B Cells**

680 Following naïve B cell isolation as described above, cells rested overnight in R20 at 37°C. For
681 transfection, Cas9/RNP complexes were prepared from TrueCut Cas9 (ThermoFisher, A36499)
682 and three sgRNAs targeting the gene of interest, and one guide targeting the non-essential cell
683 surface proxy marker CD46 to reduce DNA damage after confirming efficiency of the single CD46
684 guide (Synthego) (**Table S2**). Cells were washed and resuspended in Buffer T (Neon Transfection
685 System) as previously described (53). 400,000 cells were transfected with Cas9/RNP complexes
686 using the ThermoFisher Neon Transfection System at 2150 V, 20 ms, 1 pulse and resuspended in
687 200 µL R20 in a 96 well V-bottom plate and incubated at 37°C. One hour after transfection, cells
688 were infected with WT or LPKO virus as described above. Following infection and removal of virus,
689 cells were resuspended in 200 µL R20 and moved to a flat bottom 96 well plate.

690 Precise sample volumes were used for flow cytometry at each time point to calculate total cell
691 numbers. Two days post infection, cells were stained with anti-CD19 (Biolegend, 302212) to
692 quantify total number of cells per well for normalization. 7-, 14-, 21-, and 28-days post infection,
693 samples were stained with anti-CD46 (Biolegend, 352409) to quantify outgrowth of edited cells. As
694 infected cells expanded, fresh R20 was added in precise volumes to maintain optimal cell density
695 and allow for calculation of total cells per sample. Generation of LCLs was determined by
696 observations including cell clumping and media color change indicative of proliferation and ability
697 to passage or expand cells *in vitro*.

698 **Trans-complementation Assay**

699 This assay was performed as described previously (53). Following PBMC isolation, cord blood was
700 obtained from the Carolinas Cord Blood Ban (Pro00061264). B cells were isolated by Pan-B cell
701 isolation (STEMCELL Technologies #19554). Isolated B cells were transfected with the trans-
702 complementation plasmid (ori-P based episomal plasmid in backbone pCEP4) prior to infection
703 with LPKO or WT virus. The trans-complementation plasmid encoded tdTomato followed by a P2A
704 cleavage site, and either empty vector, wild type EBNA-LP, or mutant EBNA-LP in which the Y
705 domain leucines (Leu276, Leu780, and Leu781), of the sequence LXXXLL were modified to alanine
706 by site-directed mutagenesis (Agilent, 200521). Outgrowth of tdTomato positive cells was assess
707 by flow cytometry each week until 35 days post-infection, with compensation for the viral-encoded
708 GFP. At this final timepoint, wells were considered transformed into tdTomato positive LCLs if cells
709 were both tdTomato-expressing and contained proliferating cells passaged in culture.

710 **Prediction of Protein Structure by AlphaFold3**

711 Protein structures were predicting using the AlphaFold server (https://alphafoldserver.com) using
712 default settings. To predict the structure of a single molecular of EBNA-LP, the sequence of wild
713 type EBNA-LP (UniProt Q8AZK7) encoding 4 W domains was used for input, and the representative
714 model 0 was selected for visualization using PyMOL (98). For EBNA-LP/Sp140L (UniProt Q9H930)
715 and EBNA-LP/Sp100 (UniProt P23497) complexes, jobs were submitted with 2 molecules of each
716 protein. Model 0 for each complex was representative of predicted models and selected for
717 visualization. For complexes containing SP140L, isoform 2, which excludes the frequently skipped
718 exon 2(29), was used. For Sp100, the Sp100C isoform was used as it contains the most similar
719 domain architecture to Sp140L.

720 **Co-Immunoprecipitation in 293Ts**

721 293T cells transfected with 20 ug total DNA, using pSG5 empty vector as filler DNA. Constructs
722 expressing EBNA-LP encode synthesized cDNA (GENEWIZ) encoding four copies of the identical
723 W domain with optimized codon usage to avoid recombination and were cloned by gateway cloning
724 (ThermoFisher 11789020, and 11791020) into the vector pSG5-FLAG-Gateway (a gift from Eric
725 Johannsen) to include an N-terminal FLAG tag. DNA encoding Sp100A was from plasmid YFP-
726 Sp100A(K297A)-C1 (Addgene plasmid # 134552). The sequence encoding Sp100A was inserted
727 into the vector pCDNA3.1-HA, adding an N-terminal epitope tag, by restriction digest cloning. Site-
728 directed mutagenesis cloning was used to restore Sp100A sequence to wild type (A297K).

729 FLAG immunoprecipitations were performed as described previously (53) with 4 ug Anti-FLAG M2
730 antibody (Sigma-Aldrich, F1804). Beads were eluted in 1X LDS sample buffer (GenScript, M00676-
731 250) in lysis buffer at 37°C for 5 min followed by rotation at room temperature for 5 min.
732 Immunoprecipitation blots were imaged using primary antibodies EBNA-LP JF186 (purified in
733 house, used at a final dilution of 10 ug/uL) and Sp100 polyclonal antibody (Thermo PA5-78177,
734 1:750). Veriblot for IP Detection Reagent (HRP, abcam ab131366) was used for secondary antibody
735 at 1:1000 dilution in 5% milk in TBST. Sp100 input western blot was imaged using SuperSignal™
736 West Pico Chemiluminescent Substrate (Thermo Scientific 34080), while all other western blots
737 were imaged using SuperSignal™ West Femto Maximum Sensitivity Substrate (Thermo Scientific
738 34096).

739 **Generation of Recombinant HVS Virus**

740 A BAC clone of the HVS A11-Sac strain (which lacks the HVS transforming genes) (99) was
741 modified using RecA-mediated recombineering to replace the AgeI-BlpI fragment of dsRed1 ORF
742 with a mNeonGreen-T2A-Luciferase fusion. This generated two BAC clones (A and B) that were
743 each recombineered to delete the ORF3 open reading frame, introducing a STOP codon (alongside
744 SalI and Cla I restriction sites) after the 5th amino acid of ORF3, and deleting all but the last 237
745 nucleotides of the ORF3 coding sequence, thereby generating two independent HVS-ORF3KO
746 BACs (A-ORF3 KO and B-ORF3 KO) (as validated in **Fig. S8A**).

747
748 **HVS Virus Preparation**
749 Herpesvirus saimiri BAC is transfected into – using a peptide-lipofectin complex (100) – or
750 inoculated onto Owl Monkey kidney (OMK) cells. Supernatant is harvested when the cell
751 monolayer is largely destroyed (typically after 4-7 days) and centrifuged to remove cell debris.
752
753 **HVS Genome Quantification**
754 Virus stock was lysed by lysis buffer after DNase treatment. Then virus lysate was subjected to
755 quantify viral DNA by using Kapa SYBR Fast Universal qPCR kit (KK4602, SLS) with a pair of
756 hygromycin gene primer.
757
758 **Generation of *CD46*, *SP100*, and *SP140L* Knockout Fibroblast Cell Lines**
759 Human Foreskin Fibroblasts (HFF) and human lung fibroblast cell line MRC-5 (MRC5) were
760 maintained in Dulbecco's modified Eagle's medium (DMEM) (Gibco, Grand Island, NY, USA)
761 supplemented with 10% heat-inactivated fetal bovine serum (Gibco, Grand Island, NY, USA) at
762 37°C in a 5% CO2. For transfection, Cas9/RNP complexes were prepared in buffer T whereas
763 cells were washed and resuspended in buffer R (Neon transfection system). $2x10^5$ cells in 5 ul
764 buffer R were mixed with Cas9/RNP complexes and transfected with the neon transfection
765 system at 1650 V 10 ms, 3 pulses. Then the transfected cells were resuspended in 300 µl of 15%
766 DMEM in 12 well plate and incubated at 37°C. When cell confluency reached 80-90%, a quarter
767 of the well was stained with anti-CD46 antibody (Biolegend, 352401) to measure CD46-knockout
768 efficiency by flow cytometry as described above.
769
770 **Immunofluorescence in Fibroblast Knockout Lines**
771 HFF cells were seeded onto coverslips. At 24 hours post HVS infection, the coverslips were fixed
772 with 4% PFA for 15 minutes and permeabilized with 0.5% Triton X-100 in PBS for 15 minutes.
773 Coverslips were blocked with 10% FBS in PBS for 1 hour. The coverslips were incubated with the
774 anti-Sp100 (Invitrogen, PA5-78177) for 1 hour followed by Alexa Fluor 546 conjugated anti-rabbit
775 IgG (Invitrogen, A11071) for 1 hour. The coverslips were mounted with ProLong® Gold Antifade
776 Reagent with DAPI (Cell Signalling Technology, 8961). Images were obtained using the EVOS cell
777 imaging system.
778
779 **Knockout Screen in HVS Infected Fibroblast Cell Lines**
780 Fibroblast cells were seeded 100 ul of $3x10^5$ cells/ml triplicate wells of a white 96 well clear-
781 bottom plate. HVS WT (A and B) and HVS ORF3 KO (A-ORF3 and B-ORF3) were used to infect
782 knockout cell line at MOI of 1000 genomes/ml. After 24 hours, luciferase activity was measured
783 as a proxy for HVS transcription: cell media was removed and replaced with 50 µl fresh media, to

784 which 50 µl Steady-Glo® Luciferase Assay System reagent (Promega, E2510) was added, and
785 after 5 minutes, luminescence was measured on a FluoStar OMEGA plate reader (BMG
786 Labtech).
787
788 **Immunofluorescence in EBNA-LP trans-complemented LCLs**
789 Samples were pelleted and resuspended in 200uL of 1X PBS per slide. Cells were spun onto slides
790 using a Cytospin 4 (1000rpm for 8 min). Cells were fixed with 4% paraformaldehyde in PBS for 15
791 min at 4°C. Cells were then washed three times in 1X PBS, permeabilized in 0.5% Triton X-100 in
792 1X PBS for 15 min at RT, and blocked with 5% normal goat serum in 0.2% Triton X-100 in PBS in
793 a humid chamber for 1 hour at RT. Primary antibodies were then added to blocking buffer (JF186
794 purified from hybridoma supernatant in-house, used at a final dilution of 10 µg/µL) and incubated
795 on slides with parafilm in humid chamber overnight at 4°C. Slides were washed four times in 1X
796 PBS, incubated with secondary antibody in blocking buffer (AlexaFluor 488 goat anti-mouse IgG
797 1:250, Cat. No A11001) for 2 hours at RT and washed 4 times in 1X PBS. Slides were mounted
798 with Vectashield Vibrance Antifade mounting medium with DAPI (Vector Laboratories H-1800) and
799 imaged as Z stacks on the Olympus IX81 microscope using 60X oil objective. Images were
800 processed with Fiji (ImageJ).

801 **Knockout Validation**
802 Knockout cell lines were validated by genomic DNA (gDNA) sequencing at targeted cut sites. For
803 LPKO LCLs, the total population of LCLs (regardless of CD46 expression) was used to collect
804 samples for gDNA – as if targets have the ability to rescue LPKO infection, we expect that all
805 surviving cells are edited. Cells were pelleted and washed in PBS. gDNA was isolated (K182002,
806 ThermoFisher) and primers spanning cut sites (**Table S2**) were used to amplify region of interest.
807 gDNA from control (CD46 only) conditions were used for comparison. PCR product was sequenced
808 by Sanger Sequencing. The chromatogram files generated from sequencing were used as input
809 in the Synthego Inference of Crisper Edits Analysis tool
810 (https://www.synthego.com/products/bioinformatics/analysis), with CD46 only control cells
811 used for comparison. This was used to generate a knockout score, indicative of the percentage of
812 sequences, a direct reflection of the percentage of cells, that have indels that are highly likely to
813 result in lost expression of the targeted gene by non, either from frameshifting indels or indels larger
814 than 21 base pairs that would cause either non-sense mediated decay or loss of function mutations.
815
816 **Western Blotting**
817 Western blots were performed as previously described (53).
818
819 **Resource Availability**

All sequencing data is publicly available from the NCBI's Gene Expression Omnibus (GEO) under accession numbers: GSE282376, GSE282377, and GSE282400.

Acknowledgements

This work was supported by NIH Grant R01CA140337 (to M.A.L), MRC grant MR/L008432/1 (to R.E.W.), and F31DE031509 (to J.M.C.). We acknowledge Ashely P. Barry for reagent generation and technical assistance with the SeahorseXF assay, Elliott SoRelle for assistance with scRNAseq analysis, Gillian Horn for assistance with design of flow cytometry panels, Neha Shaw for technical assistance, Michael di Franco for pilot HVS experiments, Johanna Veldman for historic Sp140L experiments, and Nicolás Reinoso-Vizcaino for helpful discussions. We wish to thank the Duke University School of Medicine Sequencing and Genomic Technologies Shared Resource for sequencing services and the Duke Cancer Institute Flow Cytometry Facility for instrumentation.

References

1. J. I. Cohen, Herpesvirus latency. *J Clin Invest* **130**, 3361-3369 (2020).
2. T. V. Lanz *et al.*, Clonally expanded B cells in multiple sclerosis bind EBV EBNA1 and GlialCAM. *Nature* **603**, 321-327 (2022).
3. K. Bjornevik *et al.*, Longitudinal analysis reveals high prevalence of Epstein-Barr virus associated with multiple sclerosis. *Science* **375**, 296-301 (2022).
4. Y. Wong, M. T. Meehan, S. R. Burrows, D. L. Doolan, J. J. Miles, Estimating the global burden of Epstein-Barr virus-related cancers. *J Cancer Res Clin Oncol* **148**, 31-46 (2022).
5. A. Corpet *et al.*, PML nuclear bodies and chromatin dynamics: catch me if you can! *Nucleic Acids Res* **48**, 11890-11912 (2020).
6. A. Roy, A. Ghosh, Epigenetic Restriction Factors (eRFs) in Virus Infection. *Viruses* **16** (2024).
7. C. Kleijwegt *et al.*, Interplay between PML NBs and HIRA for H3.3 dynamics following type I interferon stimulus. *Elife* **12** (2023).
8. S. McFarlane *et al.*, The histone chaperone HIRA promotes the induction of host innate immune defences in response to HSV-1 infection. *PLoS Pathog* **15**, e1007667 (2019).
9. A. C. Stilp *et al.*, The chromatin remodeling protein ATRX positively regulates IRF3-dependent type I interferon production and interferon-induced gene expression. *PLoS Pathog* **18**, e1010748 (2022).
10. H. Dong *et al.*, PML Body Component Sp100A Is a Cytosolic Responder to IFN and Activator of Antiviral ISGs. *mBio* **13**, e0204422 (2022).
11. Y. E. Kim, J. H. Ahn, Positive role of promyelocytic leukemia protein in type I interferon response and its regulation by human cytomegalovirus. *PLoS Pathog* **11**, e1004785 (2015).
12. T. Alandijany *et al.*, Distinct temporal roles for the promyelocytic leukaemia (PML) protein in the sequential regulation of intracellular host immunity to HSV-1 infection. *PLoS Pathog* **14**, e1006769 (2018).
13. K. Tsai *et al.*, Viral reprogramming of the Daxx histone H3.3 chaperone during early Epstein-Barr virus infection. *J Virol* **88**, 14350-14363 (2014).
14. E. R. Albright, R. F. Kalejta, Canonical and Variant Forms of Histone H3 Are Deposited onto the Human Cytomegalovirus Genome during Lytic and Latent Infections. *J Virol* **90**, 10309-10320 (2016).
15. S. Schreiner *et al.*, Control of human adenovirus type 5 gene expression by cellular Daxx/ATRX chromatin-associated complexes. *Nucleic Acids Res* **41**, 3532-3550 (2013).

16. J. M. Cabral, H. S. Oh, D. M. Knipe, ATRX promotes maintenance of herpes simplex virus heterochromatin during chromatin stress. *Elife* **7** (2018).
17. T. S. Rai *et al.*, Histone chaperone HIRA deposits histone H3.3 onto foreign viral DNA and contributes to anti-viral intrinsic immunity. *Nucleic Acids Res* **45**, 11673-11683 (2017).
18. C. Cohen *et al.*, Promyelocytic leukemia (PML) nuclear bodies (NBs) induce latent/quiescent HSV-1 genomes chromatinization through a PML NB/Histone H3.3/H3.3 Chaperone Axis. *PLoS Pathog* **14**, e1007313 (2018).
19. D. G. Negorev, O. V. Vladimirova, G. G. Maul, Differential functions of interferon-upregulated Sp100 isoforms: herpes simplex virus type 1 promoter-based immediate-early gene suppression and PML protection from ICP0-mediated degradation. *J Virol* **83**, 5168-5180 (2009).
20. R. D. Everett, C. Parada, P. Gripon, H. Sirma, A. Orr, Replication of ICP0-null mutant herpes simplex virus type 1 is restricted by both PML and Sp100. *J Virol* **82**, 2661-2672 (2008).
21. Y. E. Kim *et al.*, Human cytomegalovirus infection causes degradation of Sp100 proteins that suppress viral gene expression. *J Virol* **85**, 11928-11937 (2011).
22. C. Habiger, G. Jager, M. Walter, T. Iftner, F. Stubenrauch, Interferon Kappa Inhibits Human Papillomavirus 31 Transcription by Inducing Sp100 Proteins. *J Virol* **90**, 694-704 (2016).
23. J. Berscheminski *et al.*, Sp100 isoform-specific regulation of human adenovirus 5 gene expression. *J Virol* **88**, 6076-6092 (2014).
24. J. S. Seeler, A. Marchio, D. Sitterlin, C. Transy, A. Dejean, Interaction of SP100 with HP1 proteins: a link between the promyelocytic leukemia-associated nuclear bodies and the chromatin compartment. *Proc Natl Acad Sci U S A* **95**, 7316-7321 (1998).
25. I. Fraschilla, K. L. Jeffrey, The Speckled Protein (SP) Family: Immunity's Chromatin Readers. *Trends Immunol* **41**, 572-585 (2020).
26. D. X. Ji *et al.*, Role of the transcriptional regulator SP140 in resistance to bacterial infections via repression of type I interferons. *Elife* **10** (2021).
27. J. S. Leu *et al.*, SP110b Controls Host Immunity and Susceptibility to Tuberculosis. *Am J Respir Crit Care Med* **195**, 369-382 (2017).
28. H. Nakamura, H. Hikichi, S. Seto, M. Hijikata, N. Keicho, Transcriptional regulators SP110 and SP140 modulate inflammatory response genes in Mycobacterium tuberculosis-infected human macrophages. *Microbiol Spectr* **12**, e0010124 (2024).
29. M. Saare *et al.*, SP140L, an Evolutionarily Recent Member of the SP100 Family, Is an Autoantigen in Primary Biliary Cirrhosis. *J Immunol Res* **2015**, 526518 (2015).
30. V. Lukashchuk, S. McFarlane, R. D. Everett, C. M. Preston, Human cytomegalovirus protein pp71 displaces the chromatin-associated factor ATRX from nuclear domain 10 at early stages of infection. *J Virol* **82**, 12543-12554 (2008).
31. J. Hwang, R. F. Kalejta, Human cytomegalovirus protein pp71 induces Daxx SUMOylation. *J Virol* **83**, 6591-6598 (2009).
32. K. Tsai, N. Thikmyanova, J. A. Wojcechowskyj, H. J. Delecluse, P. M. Lieberman, EBV tegument protein BNRF1 disrupts DAXX-ATRX to activate viral early gene transcription. *PLoS Pathog* **7**, e1002376 (2011).
33. F. Full *et al.*, Kaposi's sarcoma associated herpesvirus tegument protein ORF75 is essential for viral lytic replication and plays a critical role in the antagonization of ND10-instituted intrinsic immunity. *PLoS Pathog* **10**, e1003863 (2014).
34. F. Full, N. Reuter, K. Zielke, T. Stamminger, A. Ensser, Herpesvirus saimiri antagonizes nuclear domain 10-instituted intrinsic immunity via an ORF3-mediated selective degradation of cellular protein Sp100. *J Virol* **86**, 3541-3553 (2012).
35. M. K. Chelbi-Alix, H. de The, Herpes virus induced proteasome-dependent degradation of the nuclear bodies-associated PML and Sp100 proteins. *Oncogene* **18**, 935-941 (1999).
36. V. Lukashchuk, R. D. Everett, Regulation of ICP0-null mutant herpes simplex virus type 1 infection by ND10 components ATRX and hDaxx. *J Virol* **84**, 4026-4040 (2010).
37. H. Kang *et al.*, Inhibition of SUMO-independent PML oligomerization by the human cytomegalovirus IE1 protein. *J Gen Virol* **87**, 2181-2190 (2006).

38. P. D. Ling *et al.*, Mediation of Epstein-Barr virus EBNA-LP transcriptional coactivation by Sp100. *EMBO J* **24**, 3565-3575 (2005).
39. C. W. Echendu, P. D. Ling, Regulation of Sp100A subnuclear localization and transcriptional function by EBNA-LP and interferon. *J Interferon Cytokine Res* **28**, 667-678 (2008).
40. Y. Lu, A. Orr, R. D. Everett, Stimulation of the Replication of ICP0-Null Mutant Herpes Simplex Virus 1 and pp71-Deficient Human Cytomegalovirus by Epstein-Barr Virus Tegument Protein BNRF1. *J Virol* **90**, 9664-9673 (2016).
41. R. D. Everett, A. J. Bell, Y. Lu, A. Orr, The replication defect of ICP0-null mutant herpes simplex virus 1 can be largely complemented by the combined activities of human cytomegalovirus proteins IE1 and pp71. *J Virol* **87**, 978-990 (2013).
42. Y. Lu, R. D. Everett, Analysis of the functional interchange between the IE1 and pp71 proteins of human cytomegalovirus and ICP0 of herpes simplex virus 1. *J Virol* **89**, 3062-3075 (2015).
43. D. G. Negorev, O. V. Vladimirova, A. Ivanov, F. Rauscher, 3rd, G. G. Maul, Differential role of Sp100 isoforms in interferon-mediated repression of herpes simplex virus type 1 immediate-early protein expression. *J Virol* **80**, 8019-8029 (2006).
44. A. Szymula *et al.*, Epstein-Barr virus nuclear antigen EBNA-LP is essential for transforming naive B cells, and facilitates recruitment of transcription factors to the viral genome. *PLoS Pathog* **14**, e1006890 (2018).
45. Q. Peng *et al.*, Phase Separation of Epstein-Barr Virus EBNA2 and Its Coactivator EBNALP Controls Gene Expression. *J Virol* **94** (2020).
46. S. Harada, E. Kieff, Epstein-Barr virus nuclear protein LP stimulates EBNA-2 acidic domain-mediated transcriptional activation. *J Virol* **71**, 6611-6618 (1997).
47. E. M. McCann, G. L. Kelly, A. B. Rickinson, A. I. Bell, Genetic analysis of the Epstein-Barr virus-coded leader protein EBNA-LP as a co-activator of EBNA2 function. *J Gen Virol* **82**, 3067-3079 (2001).
48. F. Nitsche, A. Bell, A. Rickinson, Epstein-Barr virus leader protein enhances EBNA-2-mediated transactivation of latent membrane protein 1 expression: a role for the W1W2 repeat domain. *J Virol* **71**, 6619-6628 (1997).
49. R. Peng, S. C. Moses, J. Tan, E. Kremmer, P. D. Ling, The Epstein-Barr virus EBNA-LP protein preferentially coactivates EBNA2-mediated stimulation of latent membrane proteins expressed from the viral divergent promoter. *J Virol* **79**, 4492-4505 (2005).
50. A. Yokoyama *et al.*, Identification of major phosphorylation sites of Epstein-Barr virus nuclear antigen leader protein (EBNA-LP): ability of EBNA-LP to induce latent membrane protein 1 cooperatively with EBNA-2 is regulated by phosphorylation. *J Virol* **75**, 5119-5128 (2001).
51. D. Portal *et al.*, EBV nuclear antigen EBNALP dismisses transcription repressors NCoR and RBPJ from enhancers and EBNA2 increases NCoR-deficient RBPJ DNA binding. *Proc Natl Acad Sci U S A* **108**, 7808-7813 (2011).
52. D. Portal, A. Rosendorff, E. Kieff, Epstein-Barr nuclear antigen leader protein coactivates transcription through interaction with histone deacetylase 4. *Proc Natl Acad Sci U S A* **103**, 19278-19283 (2006).
53. J. M. Cable, N. M. Reinoso-Vizcaino, R. E. White, M. A. Luftig, Epstein-Barr virus protein EBNA-LP engages YY1 through leucine-rich motifs to promote naive B cell transformation. *PLoS Pathog* **20**, e1011950 (2024).
54. E. D. SoRelle *et al.*, Time-resolved transcriptomes reveal diverse B cell fate trajectories in the early response to Epstein-Barr virus infection. *Cell Rep* **40**, 111286 (2022).
55. P. A. Nikitin *et al.*, An ATM/Chk2-mediated DNA damage-responsive signaling pathway suppresses Epstein-Barr virus transformation of primary human B cells. *Cell Host Microbe* **8**, 510-522 (2010).
56. K. McFadden *et al.*, Metabolic stress is a barrier to Epstein-Barr virus-mediated B-cell immortalization. *Proc Natl Acad Sci U S A* **113**, E782-790 (2016).
57. S. Beer *et al.*, EBNA2-EBF1 complexes promote MYC expression and metabolic processes driving S-phase progression of Epstein-Barr virus-infected B cells. *Proc Natl Acad Sci U S A* **119**, e2200512119 (2022).

58. R. Nakagawa, D. P. Calado, Positive Selection in the Light Zone of Germinal Centers. *Front Immunol* **12**, 661678 (2021).
59. E. Playoust, R. Remark, E. Vivier, P. Milpied, Germinal center-dependent and -independent immune responses of tumor-infiltrating B cells in human cancers. *Cell Mol Immunol* **20**, 1040-1050 (2023).
60. E. Forte, M. A. Luftig, MDM2-dependent inhibition of p53 is required for Epstein-Barr virus B-cell growth transformation and infected-cell survival. *J Virol* **83**, 2491-2499 (2009).
61. A. B. Keenan *et al.*, ChEA3: transcription factor enrichment analysis by orthogonal omics integration. *Nucleic Acids Res* **47**, W212-W224 (2019).
62. J. Liao *et al.*, CENPA functions as a transcriptional regulator to promote hepatocellular carcinoma progression via cooperating with YY1. *Int J Biol Sci* **19**, 5218-5232 (2023).
63. D. G. Patterson *et al.*, An IRF4-MYC-mTORC1 Integrated Pathway Controls Cell Growth and the Proliferative Capacity of Activated B Cells during B Cell Differentiation In Vivo. *J Immunol* **207**, 1798-1811 (2021).
64. Y. Ma *et al.*, CRISPR/Cas9 Screens Reveal Epstein-Barr Virus-Transformed B Cell Host Dependency Factors. *Cell Host Microbe* **21**, 580-591 e587 (2017).
65. P. Li *et al.*, BATF-JUN is critical for IRF4-mediated transcription in T cells. *Nature* **490**, 543-546 (2012).
66. P. R. Arnold *et al.*, Suppression of FOXP3 expression by the AP-1 family transcription factor BATF3 requires partnering with IRF4. *Front Immunol* **13**, 966364 (2022).
67. E. Akidil *et al.*, Highly efficient CRISPR-Cas9-mediated gene knockout in primary human B cells for functional genetic studies of Epstein-Barr virus infection. *PLoS Pathog* **17**, e1009117 (2021).
68. J. Abramson *et al.*, Accurate structure prediction of biomolecular interactions with AlphaFold 3. *Nature* **630**, 493-500 (2024).
69. R. J. Whitley, "Herpesviruses" in Medical Microbiology, S. Baron, Ed. (Galveston (TX), 1996).
70. J. Hwang, R. F. Kalejta, Proteasome-dependent, ubiquitin-independent degradation of Daxx by the viral pp71 protein in human cytomegalovirus-infected cells. *Virology* **367**, 334-338 (2007).
71. R. T. Saffert, R. F. Kalejta, Human cytomegalovirus gene expression is silenced by Daxx-mediated intrinsic immune defense in model latent infections established in vitro. *J Virol* **81**, 9109-9120 (2007).
72. T. Gunther, S. Schreiner, T. Dobner, U. Tessmer, A. Grundhoff, Influence of ND10 components on epigenetic determinants of early KSHV latency establishment. *PLoS Pathog* **10**, e1004274 (2014).
73. N. Lehming, A. Le Saux, J. Schuller, M. Ptashne, Chromatin components as part of a putative transcriptional repressing complex. *Proc Natl Acad Sci U S A* **95**, 7322-7326 (1998).
74. M. Lachner, D. O'Carroll, S. Rea, K. Mechtler, T. Jenuwein, Methylation of histone H3 lysine 9 creates a binding site for HP1 proteins. *Nature* **410**, 116-120 (2001).
75. D. Pich *et al.*, First Days in the Life of Naive Human B Lymphocytes Infected with Epstein-Barr Virus. *mBio* **10** (2019).
76. S. Chen *et al.*, Crucial Roles of RSAD2/viperin in Immunomodulation, Mitochondrial Metabolism and Autoimmune Diseases. *Inflammation* 10.1007/s10753-024-02076-5 (2024).
77. K. Honarmand Ebrahimi, J. Vowles, C. Browne, J. McCullagh, W. S. James, ddhCTP produced by the radical-SAM activity of RSAD2 (viperin) inhibits the NAD(+) -dependent activity of enzymes to modulate metabolism. *FEBS Lett* **594**, 1631-1644 (2020).
78. A. R. Dinasarapu *et al.*, A combined omics study on activated macrophages--enhanced role of STATs in apoptosis, immunity and lipid metabolism. *Bioinformatics* **29**, 2735-2743 (2013).
79. M. Hedl, J. Yan, C. Abraham, IRF5 and IRF5 Disease-Risk Variants Increase Glycolysis and Human M1 Macrophage Polarization by Regulating Proximal Signaling and Akt2 Activation. *Cell Rep* **16**, 2442-2455 (2016).

80. D. M. Heery, E. Kalkhoven, S. Hoare, M. G. Parker, A signature motif in transcriptional co-activators mediates binding to nuclear receptors. *Nature* **387**, 733-736 (1997).
81. C. H. Ludwig *et al.*, High-throughput discovery and characterization of viral transcriptional effectors in human cells. *Cell Syst* **14**, 482-500 e488 (2023).
82. N. E. Davey *et al.*, Attributes of short linear motifs. *Mol Biosyst* **8**, 268-281 (2012).
83. L. Simonetti, J. Nilsson, G. McInerney, Y. Ivarsson, N. E. Davey, SLiM-binding pockets: an attractive target for broad-spectrum antivirals. *Trends Biochem Sci* **48**, 420-427 (2023).
84. J. A. DeCaprio, The role of the J domain of SV40 large T in cellular transformation. *Biologicals* **27**, 23-28 (1999).
85. T. Sternsdorf, K. Jensen, B. Reich, H. Will, The nuclear dot protein sp100, characterization of domains necessary for dimerization, subcellular localization, and modification by small ubiquitin-like modifiers. *J Biol Chem* **274**, 12555-12566 (1999).
86. R. D. Everett, C. Boutell, C. McNair, L. Grant, A. Orr, Comparison of the biological and biochemical activities of several members of the alphaherpesvirus ICP0 family of proteins. *J Virol* **84**, 3476-3487 (2010).
87. E. J. Aird, Rabl, J., Knuesel, T., Scherpe, L., Boehringer, D., Corn, J.E., SP110 sequestration of SP100 protects against toxic filaments during innate immune signaling. *bioRxiv preprint* (2024).
88. G. Monaco *et al.*, RNA-Seq Signatures Normalized by mRNA Abundance Allow Absolute Deconvolution of Human Immune Cell Types. *Cell Rep* **26**, 1627-1640 e1627 (2019).
89. A. Isaac, K. W. Wilcox, J. L. Taylor, SP100B, a repressor of gene expression preferentially binds to DNA with unmethylated CpGs. *J Cell Biochem* **98**, 1106-1122 (2006).
90. X. Zhang, D. Zhao, X. Xiong, Z. He, H. Li, Multifaceted Histone H3 Methylation and Phosphorylation Readout by the Plant Homeodomain Finger of Human Nuclear Antigen Sp100C. *J Biol Chem* **291**, 12786-12798 (2016).
91. C. L. Johnson, M. Gale, Jr., CARD games between virus and host get a new player. *Trends Immunol* **27**, 1-4 (2006).
92. S. Mehta *et al.*, Maintenance of macrophage transcriptional programs and intestinal homeostasis by epigenetic reader SP140. *Sci Immunol* **2** (2017).
93. H. Amatullah *et al.*, Epigenetic reader SP140 loss of function drives Crohn's disease due to uncontrolled macrophage topoisomerases. *Cell* **185**, 3232-3247 e3218 (2022).
94. M. M. Ba Abdullah *et al.*, Heterogeneity of the Epstein-Barr Virus (EBV) Major Internal Repeat Reveals Evolutionary Mechanisms of EBV and a Functional Defect in the Prototype EBV Strain B95-8. *J Virol* **91** (2017).
95. R. Satija, J. A. Farrell, D. Gennert, A. F. Schier, A. Regev, Spatial reconstruction of single-cell gene expression data. *Nat Biotechnol* **33**, 495-502 (2015).
96. G. Yu, L. G. Wang, Y. Han, Q. Y. He, clusterProfiler: an R package for comparing biological themes among gene clusters. *OMICS* **16**, 284-287 (2012).
97. V. K. Mootha *et al.*, PGC-1alpha-responsive genes involved in oxidative phosphorylation are coordinately downregulated in human diabetes. *Nat Genet* **34**, 267-273 (2003).
98. L. Schroedinger (The PyMOL Molecular Graphics System, Version 3.1.
99. R. E. White, M. A. Calderwood, A. Whitehouse, Generation and precise modification of a herpesvirus saimiri bacterial artificial chromosome demonstrates that the terminal repeats are required for both virus production and episomal persistence. *The Journal of general virology* **84**, 3393-3403 (2003).
100. R. E. White *et al.*, Functional delivery of large genomic DNA to human cells with a peptide-lipid vector. *The Journal of Gene Medicine* **5**, 883-892 (2003).